SYNTHESIS OF NITROGEN-DOPED GRAPHENE QUANTUM DOTS AND ITS ANTIBACTERIAL PROPERTY

WONG KA KIT

M.Phil

The Hong Kong Polytechnic University

2018

The Hong Kong Polytechnic University

Department of Applied Physics

Synthesis of Nitrogen-Doped Graphene Quantum Dots and Its Antibacterial Property

Wong Ka Kit

A thesis submitted in partial fulfillment of the requirements

for the degree of Master of Philosophy

August 2017

Certificate of originality

I hereby declare that this thesis is my own work and that, to the best of my knowledge and belief, it reproduces no material previously published or written, nor material that has been accepted for the award of any other degree or diploma, except where due acknowledgment has been made in the text.

_____ (Signature)

Wong Ka Kit (Name of student)

Abstract

Bacterial infection presents a serious global challenge to human health nowadays, especially with increasing bacterial resistance. Graphene quantum dots (GQDs) are nano-scale graphitic fragments with sp^2 hybridized carbon atoms edged with heteroatomic functional groups. As a new-age nanoparticle, it is a potential candidate for new antibacterial agent due to its low cytotoxicity and high chemical stability, compared to other nanoparticles. Most importantly, its passivation can be crafted to make it suitable in antibacterial and optoelectronic applications.

This work aims to fabricate nitrogen-doped GQDs (N-GQDs) and investigate its antibacterial effect. N-GQDs were synthesized by microwave-assisted hydrothermal synthesis using p-phenylenediamine as a precursor. The as-prepared N-GQDs solution underwent column chromatography and was separated into four fractions. Each fraction of the N-GQD solution showed distinguishable photoluminescence (PL) properties. The fractions were named according to their PL peak emission color, i.e. green (g-GQDs), yellow (y-GQDs), orange (o-GQDs) and red (r-GQDs).

The GQDs samples showed an absorption peak at 245 nm, indicating π-π^* transitions of C=C bonds. Transmission electron microscopy (TEM) studies showed that the GQDs exhibited graphitic structure with an average size of ~ 2.5 nm. X-ray

photoelectron spectroscopy (XPS) showed an increase in nitrogen content (from 9.1% to 16.2%) with a decrease in oxygen content (from 13.5% to 7.2%) according to the following order: g-GQDs, y-GQDs, o-GQDs and r-GQDs.

Gram-positive *S. aureus* and gram-negative *E. coli* were treated with the four GQD fractions in order to investigate their antibacterial abilities. Minimal inhibitory concentration (MIC) was measured to evaluate the antibacterial power of the GQDs. The antibacterial effect of the GQDs was found to be more effective in *S. aureus* than in *E. coli*. The MIC value towards *S. aureus* decreased from g-GQDs (171 μg/mL) to r-GQDs (43 μg/mL), indicating the increasing trend in antibacterial power as the nitrogen content increase.

Acknowledgements

I would like to thank my supervisor Prof. S. P. Lau for his great support and professional advice in my research. It is my honor to be under Prof. Lau's valuable supervision. It is also my pleasure to work with Dr. Z. T. Fan in this project. I would like to express my thank to Dr. Vincent Chan and Dr. Hardy Lui for their experienced guidance in experiments.

I am also grateful to have Dr. S. Chen and Ms. H. L. Po from the Department of Applied Biology and Chemical Technology in The Hong Kong Polytechnic University as my collaborators. The biological test cannot be successful without their insight and guidance. Furthermore, the training on liquid chromatography by Mr. Cheong Wing Lam is highly appreciated.

I would also like to express my thank to my senior research groupmates Dr. C. M. Luk and Mr. C. H. Mak for their patient guidance and discussion with me.

Last but not least, I would like to take this chance to appreciate the continuous support and understanding from my parent and my girlfriend, Ms. Sonia Li, especially at the toughest moments during my study period.

Table of Content

List of figures and tables

Chapter 1 Introduction

1.1 Background

Nanostructure is a family of structures with molecular or structural dimension in nanometer scale. Quantum confinement occurs when the spatial dimension is comparable to the de Broglie wavelength of charge carrier, restricting the movement of carriers and turning the energy spectrum from continuous to discrete. Thanks to the quantum confinement effect, quantum dots (QDs) have attracted great research interest globally. Many researches on optical and electronic properties of QDs were carried out and various fabrication methods were developed. Semiconductor QDs like CdS, ZnS and TiO_2 are outstanding examples, as they possess high carrier mobility and optical absorption. However, the use of toxic and heavy-metal based precursors lead to a great environmental and health issue.

As a family of nanostructure, graphene quantum dots (GQDs) have ignited tremendous research interest in recent years. GQDs is a kind of graphitic nanoparticles with dimension in nanometer scale, displaying typical size and excitation wavelength dependent photoluminescence (PL). The surface moieties give them an excellent solubility and ability to be further functionalized with a wide variety of organic compounds, in order to fit the applications. GQDs are widely applied in optoelectronic

devices, thanks to its fascinating optical absorption and emission properties. [1-11] For example, its high absorbance in UV range make it a suitable candidate for light harvesting in a photodetector. [2] Also, GQDs were employed in solar cells to improve its efficiency by the downconversion of photons [12]

Because of the availability of carbon atom to bond with a variety of atoms like nitrogen and oxygen, its surface can be passivated with functional groups. Fabrication process and precursors determine the surface functional group attached to GQDs. The functional groups affect the energy states of GQDs, and hence the electronic and optical properties.

From the view of environmental and health concern, GQDs are superior to other QDs, because of its low toxicity. Other QDs usually contain metal atoms, which will release toxic metal ions. On the other hand, GQDs has a stable carbon frame and passivated groups, making it safe to be injected into living bodies. Also, the flexibility in surface passivation gives GQDs a large freedom to be tailor-made for the antibacterial purpose. [1, 13-19]

GQDs' antibacterial property does have room for improvement, as there have been few reports studied the antibacterial property of GQDs. For nitrogen functionalized GQDs, an advantage of no requirement on light exposure gives it a great potential for clinical application, as absorption of photons by human tissue need not to be considered.

Also, compared to complicated synthetic route of conventional drugs, bottom up hydrothermal synthesis of N-GQDs is a low-cost and facile process, enabling a large-scale production.

It is found that the cationic surface of N-GQDs interacts with bacteria species to achieve antibacterial effect. [73,74,77,78] However, there has been no reports focusing on the relationship between GQDs nitrogen content and its antibacterial effect. In this thesis, nitrogen-doped GQDs were synthesized and separated into fractions with different nitrogen content by running liquid chromatography. Their inhibiting effect on *S. aureus* is found to be related to GQDs nitrogen content.

1.2 Scope of this project

N-GQDs were fabricated using microwave-assisted hydrothermal technique, with *p-phenylenediamine* as a precursor. Column chromatography was carried out to separate the GQD solution into four fractions with different polarities. The structural and optical properties of the GQDs in each fraction was characterized. Drug-resistive bacteria *S. aureus* and *E. coli* were incubated with the GQDs fractions to examine the bacterial inhibiting power of GQDs.

In chapter 2, brief information and development of GQDs are described. Common synthesis routes and properties are introduced.

In chapter 3, experimental details of the GQDs are described. The characterization process like transmission electron microscopy (TEM), photoluminescence (PL) and X-ray photoelectron spectroscopy (XPS) are included.

In chapter 4, details and methodology of column chromatography are described. Liquid chromatography (LC) and thin-plate chromatography (TLC) are included.

In chapter 5, the characterization results are described. Optical and physical properties of GQDs are shown.

In chapter 6, the biological properties of the GQDs are described.

Chapter 2 Graphene Quantum Dots

Graphene quantum dots (GQDs) refers to nanoparticles formed by a few layers of graphene, with size less than 100 nanometers.[20] As an abundant element on earth, carbon forms a variety of structures like carbon nanotubes, diamonds and fullerene. Since single layer graphene was obtained by tapes peeling [21], graphene has attracted awareness of researcher because of its outstanding electrical and mechanical properties. Graphene is a zero-bandgap material, which limits its application in optoelectronics as it is almost impossible to observe photoluminescence (PL). However, thanks to its high mobility, graphene has a very large exciton Bohr radius, allowing quantum confinement effect to take place. With the decreasing in size of the graphene layer, the bandgap of graphene could be opened. By controlling the size of graphene, its bandgap could be tuned to be semiconductor-like. For a small piece of graphene quantum dot in nano-scale, the bandgap can be opened to a few electron-volt. [22] The opening of bandgap gives GQDs PL, which is a fascinating optical property. Most of the GQDs exhibited down-conversion PL, [4, 23-25]

Besides GQDs, there are also some other zero-dimension carbon-based fluorescent nanomaterials like diamond nanocrystals and carbon dots. Diamond nanocrystal consists of a high carbon content with residual atoms like nitrogen and oxygen. [20] It possesses a sp^3 hybridization, with a tiny amount of sp^2 graphitic carbon layer on the

surface. GQDs could be regarded as a member of carbon dots (CDs) family, while there are some differences between them. Amorphous CDs can be prepared by various carbon precursors, while GQDs are usually prepared by graphene like precursors. CDs have similar optical properties as GQDs, while it has a lower mobility than GQDs because of the amorphous structure. CDs has advantages similar to GQDs like size and surface tunable luminescence, low cytotoxicity and high photostability, enabling its application in optoelectronic and biomedical fields.

2.1 Synthesis Method

GQDs can be synthesized by various methods. The synthesis method can be divided into two major categories, which are top-down and bottom-up method.

2.1.1 Top-down method

Top-down methods refer to the processes where GQDs are formed by cutting or cleaving of large carbon material like graphene oxide (GO). Top-down routes can be divided into physical and chemical process.

Ultrasonic synthesis is one of the physical top-down routes. Large carbon precursors like graphene were broken into small fragments under ultrasonic treatment, forming GQDs as a product.[26] For example, treating GO with $KMnO_4$ as an oxidizing

agent under ultrasonic process for 4 hours successfully synthesized GQDs. [27]

Most of the top-down methods are chemical processes. Defects are introduced to the large carbon material so that the cleavage of large carbon materials can take place at the defect sites. Acidic exfoliation is a typical method for top-down GQDs synthesis. GO are broken down into smaller parts under an acidic environment, while heat is needed in most of the cases. Acidic environment enhanced the uniformity of GQDs product. [28] For example, Peng *et al.* reported that dispersing carbon fiber into concentrated acid under sonication for two hours and stirring for 24 hours with various temperatures resulted in GQDs with different sizes and PL emission properties.[29] Acidic exfoliation provides a large space for researchers to tailor-made GQDs with desired properties by varying experimental parameters like reaction temperatures, choice of acid and time of exfoliation.

Besides, top-down hydrothermal cutting of graphene precursors is also viable to fabricate GQDs. Usually, strong alkali like NaOH and ammonia are applied as scissors for cutting the precursor. For example, amino-functionalized GQDs with specific edges and sizes were synthesized by hydrothermal cutting of oxidized graphene sheets, [30] as illustrated in Figure 2.1.

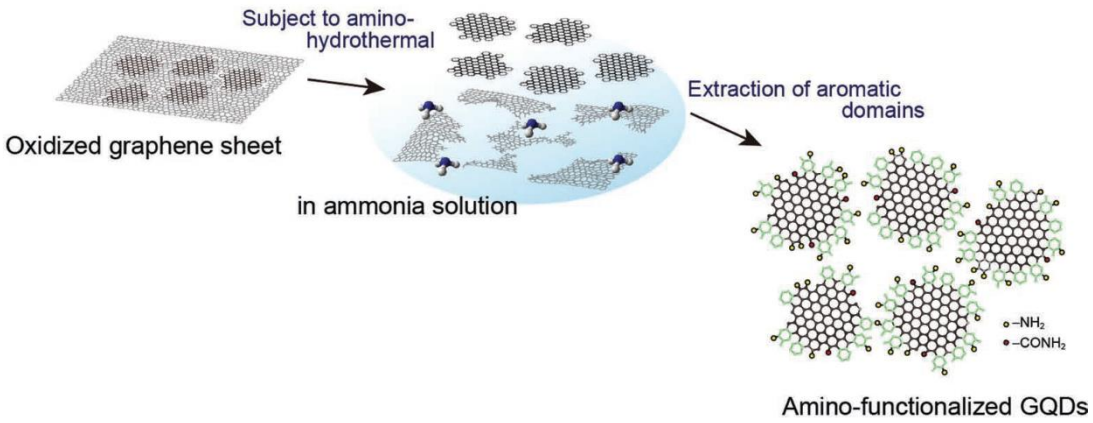

Figure 2.1 Process of hydrothermal top-down cleavage of oxidized graphene sheets by ammonia. [30]

Electrochemical method is also a top-down process to fabricate GQDs. Carbon based materials like graphite and carbon nanotubes (CNTs) were used as electrodes to undergo electrolysis.[31-33] Applying electric potential to the electrodes allows oxidation of C-C bond and water molecules to occur. Free radicals generated by oxidation of water molecules act as the scissor to speed up cleaving process of electrodes.

2.1.2 Bottom-up method

Bottom-up methods are processes where GQDs are formed by nucleation of small carbon-containing precursors. It was reported that C_{60} molecule can act as a starting material for formation of GQDs. By applying ruthenium as a catalyst, the cage of C_{60} can be opened. Due to the strong interaction between C_{60} and ruthenium, surface vacancies are formed on Ru single crystal and fragments of C_{60} are able to embed in the vacancy. Carbon clusters then diffuse back to solvent and aggregate to form GQDs. [34]

Besides C_{60}, researchers have been trying to use a variety of carbon containing molecules for hydrothermal synthesis of GQDs. For example, glucose could be used as starting material to fabricate GQDs by hydrothermal method.[23, 35] Tang *et al.* reported a facile microwave assisted hydrothermal method for treating aqueous glucose solution under microwave heating for a few minutes. During the high-pressure heating process, glucose molecules are dehydrated to sp^2 hybridization structure. With an increase of heating time, GQDs with a larger diameter are formed by continuous nucleation of dehydrated glucose molecules, as shown in Figure 2.2. [23] Because of the high pressure throughout the heating process, the sp^2 hybridized carbon structure tends to form a crystalline structure.

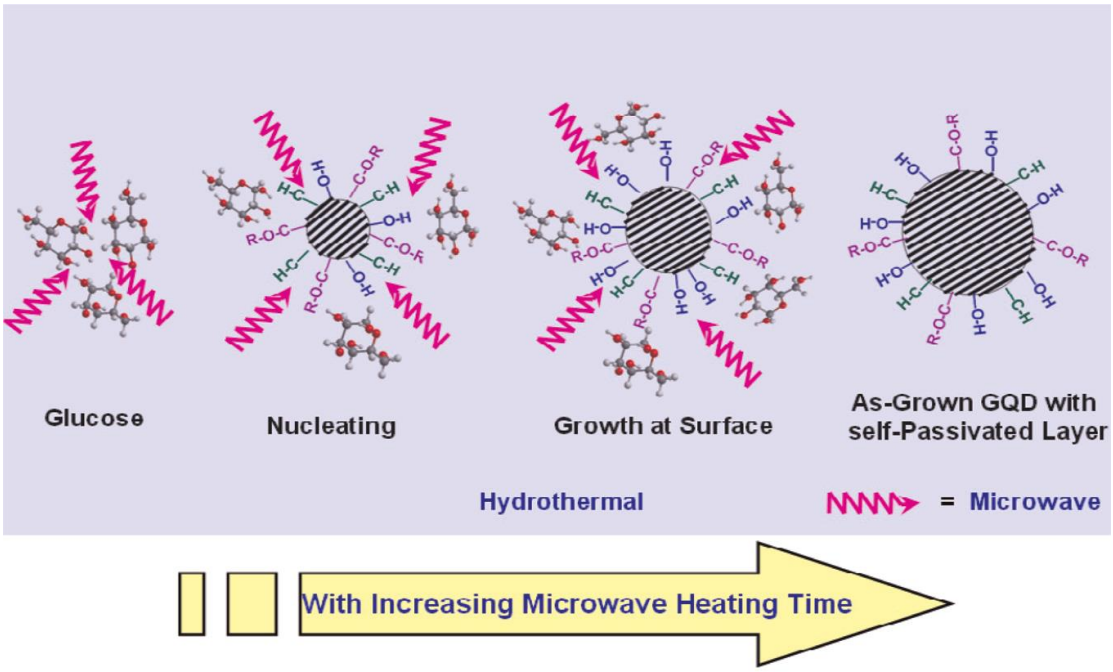

Figure 2.2 Formation of GQD particle from nucleation of glucose molecules under high-pressure microwave heating. [23]

2.3 Structural properties

The size of GQDs is closely related to the preparation method, while it is independent of the precursors chosen. By tuning experimental conditions, size and height of GQDs can be controlled. For example, for hydrothermal synthesis, the increase in heating time provides a longer duration for precursor nucleation, and hence GQDs with larger diameter are produced. [23] Figure 2.3 shows a single GQD nanoparticle fabricated by hydrothermal process of aqueous glucose solution under TEM characterization. It has a diameter of 7 nm, and a clear lattice fringe can be observed.

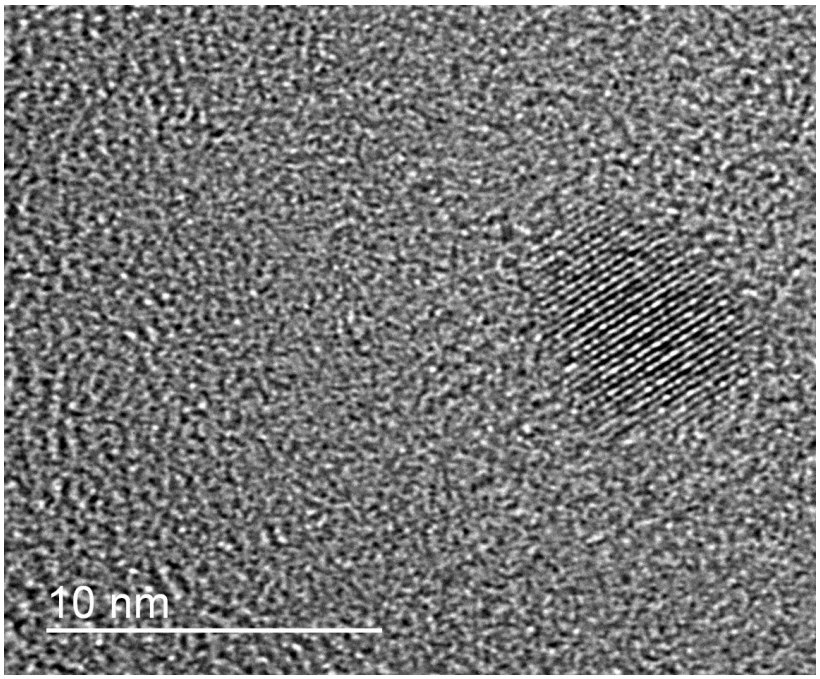

Figure 2.3 TEM image of a GQD fabricated by hydrothermal process of glucose solution.

Because of the interaction of precursors and other species like solvent molecules during the fabrication process, GQDs prepared are usually oxidized, while the oxidizing degree depends on experimental condition and choice of chemical involved. Oxygen functional group like carbonyl, carboxylic and epoxy group can be found in the GQDs by Fourier transform infrared (FTIR) and X-ray photoelectron spectroscopy (XPS). If other species like nitrogen containing molecules are involved in the fabrication process (where it can either be added in a one-step process or treated during post-processing), GQDs can be passivated depending on the atomic component of the molecule. For example, Sekiya *et al.* demonstrated the post-synthesis modification of GQDs by applying 4-propynyloxybenzyl group. [36]

2.4 Optical properties

Usually, GQDs show a strong absorption in UV region, with a tail extending to visible region. Typical absorption spectra were shown in Figure 2.4. The first peak is between 200 nm to 260 nm because of the π-π* transition of graphene structure. Another shoulder at position longer than 260 nm is due to n-π* transition of C=O bond. The actual peak and shoulder position strongly depends on starting material and fabrication method. [37-39] GQDs fabricated by top-down synthesis exhibits size dependent optical absorption due to quantum confinement effect. [29] However, there are exceptions that some bottom-up fabricated GQDs exhibit a size independent absorption peak. [23]

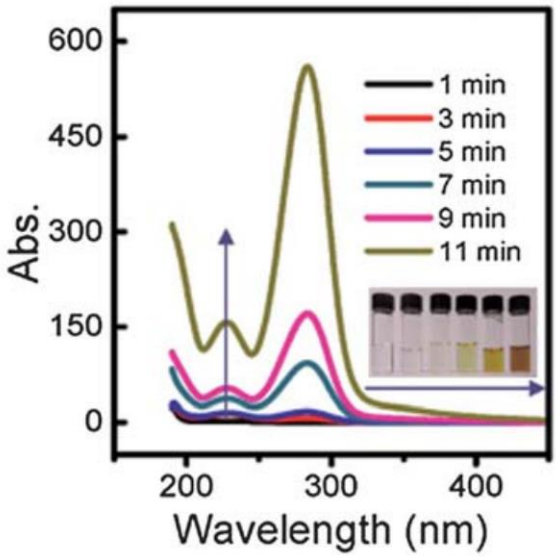

Figure 2.4 Typical absorption spectra of GQDs. GQDs were fabricated by microwave-assisted hydrothermal synthesis under different heating times. [23]

PL is one of the most significant features of GQDs. GQDs with various PL emission spectra ranging from visible to near-infrared have been reported. [4, 23, 40-42] However, the exact mechanism of PL has not been fully explained, but there are a few proposed mechanisms, like zigzag edge of graphene planes, emissive traps, surface functional groups and quantum confinement effect, to account for the PL origin. [43-46] Similar to absorption property, PL of GQDs is strongly dependent on fabrication method, experimental condition and choice of precursors. In general, PL of GQDs is mainly from intrinsic and defect state emission. [47] They may compete or contribute to the PL property together. Das *et al.* demonstrated steady state fluorescence with single particle studies of undoped and N-doped GQDs with an excitation wavelength of 488, 561 and 640 nm. [24] Under each excitation, single particle PL was examined. It was found that each GQD particle is capable of single emission band only under the same excitation. Because of variation in GQD during the fabrication process, each individual GQD possess slightly different PL properties.

In general, most GQDs exhibit excitation dependence PL, where their PL emission depends on excitation wavelength. Emission band red-shift while excitation wavelength increases. Excitation dependent PL behaviors reflects the distribution of different emissive sites on GQDs. [23, 24, 43] On the other hand, excitation independent PL can be found in uniform GQDs with a smaller variation in size and emissive sites. [9, 48]

Surface functionalization plays an important role on PL of GQDs. Because of the availability of carbon atom to bond with a variety of atoms like nitrogen and oxygen, its surface can be passivated with functional groups. Fabrication process and precursors determine the surface functional group attached onto GQDs, where the functional groups affect the energy states of GQDs, and hence the optical properties. For example, passivating GQDs with alkylamines replacing initial oxygen functional group change the PL emission color. [47] Introducing functional group onto the surface of GQDs alters the energy state, and hence the PL of the GQDs are affected. [40] Generally, electron-donating groups raised the highest occupied molecular orbital (HOMO) while electron-withdrawing group lowers the lowest unoccupied molecular orbital (LUMO) [40, 49] Many literatures showed that surface functionalization greatly influences the PL properties of GQDs.[23, 25, 50, 51]

Doping heteroatoms into GQDs tunes their intrinsic properties, and hence the PL property. Nitrogen atom is widely applied as a dopant in carbon based material, as it has similar atomic size and five valence electrons for bonding with carbon atoms. By altering the doping concentration of N, the tunable emission of CDs was demonstrated. [52]

2.5 Antibacterial properties of nanoparticles

Antibacterial activity is related to compounds or species that locally kill bacteria or inhibit their growth without being toxic to surrounding tissue. [53] Nowadays, bacterial infection is a serious global health issue, causing risk to patients' healthcare. Overuse of antimicrobial and mutation of bacteria are accelerating the development of bacteria's antimicrobial resistance, reducing the effect of traditional antibiotics. [54] New development of resistance mechanism has been emerging and spreading globally, causing threats to our conventional method to treat common infection and illness. Also, without effective antibiotics, major surgery and cancer chemotherapy cannot be compromised. We are reaching a post-antibiotic era that bacteria are developing multidrug-resistance (MDR) while there is a lack of new antibiotics to kill them. [55] Therefore, there is a need to develop new antibiotics or drug to treat MDR bacteria. Nanoparticles (NP), with an advantage of a high surface to volume ratio, offer a high flexibility in crafting its chemical, electrical and optical properties, and hence can be tuned to effectively deal different antibacterial strain. Nanoparticles like silver NP and semiconductor NP were developed as new-age antibacterials. They provide an effective antibacterial property, while the high cytotoxicity and low photostability are remained to be obstacles.

The exact mechanism of antibacterial ability of NPs is not completely understood yet. Usually, NPs are attached to the bacteria membrane by electrostatic interaction, and further interrupting the integrity of the membrane in various ways. NP toxicity towards bacteria is dependent on its atomic composition, surface modification and intrinsic property, and the type of bacteria. One of the common antibacterial mechanism is dealing oxidative stress by the generation of reactive oxygen species (ROS). Excitons are created when semiconductor NPs like TiO_2 [56, 57] and ZnO [58, 59] absorb photons. Figure 2.5 shows a schematic diagram of the generation of ROS by nanoparticle. Due to the negative electron affinity, the excited electrons are attracted to the NP surface, turning surrounding water and oxygen molecules into reactive oxygen species like oxygen singlets and free radicals, dealing oxidative stress to bacteria species. There have been reports about the antibacterial property of GQDs or CDs, as shown in Table 2.1. CDs exhibit a great advantage of low long-term cytotoxicity than most of other nanoparticles.

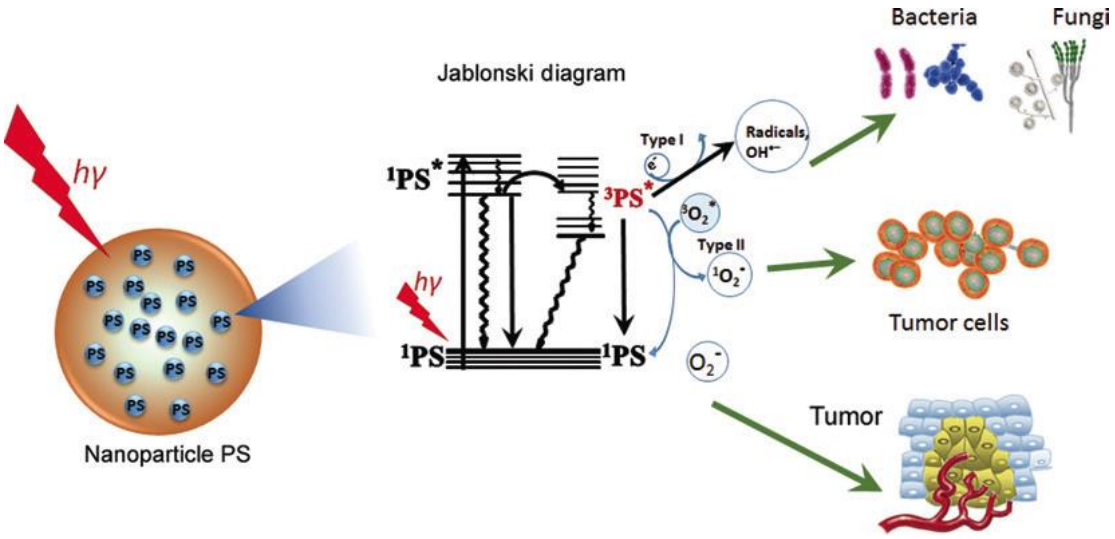

Figure 2.5 Schematic diagram showing the generation of ROS by nanoparticle photosensitizers (PSs) for antibacterial and cancer therapy. [60]

So far, most of the reported antibacterial CDs were exhibiting photo-excitation enhanced antibacterial or anti-cancer-cell property. [61-66] When the CDs absorb photons, reactive oxygen species are generated to attain the killing effect to target cells. Exact species of ROS can be characterized by various tests. For example, free radicals can be tested by electron spin resonance (ESR), while oxygen singlets can be tested by quenching of absorption of disodium 9,10-anthracen-dipropionic acid (Na_2-ADPA). For this kind of GQD species, they are commonly made from top-down method. This can be related to the reservation of graphene lattice structure of precursors, while the graphitic structure enhances its electronic mobility, enabling the creation of excitons to generate ROS. ROS can induce oxidative stress to bacteria cellular structure like cell membrane, DNA and mitochondria, resulting in cell deaths. [53]

Fabrication Method	**Starting Material**	**Target**	**Light Source**	**Reference**
Acidic exfoliation	GO	*E. coli*	800 nm laser	[61]
Acidic exfoliation	GO	*E. coli*	670 nm laser	[62]
Acidic Exfoliation	Carbon nanopowder	*E. coli*	36 W light bulb in light box	[65]
Solvothermal Method	Glycerol and AEEA	*S. aureus*, *M. luteus* and *B. subtilis*	No light is needed	[67]
Hydrothermal method	Glucose and PEI	*E. coli* and *S. aureus*	No light is needed	[68]

Table 2.1 A utilization summary of GQDs in antibacterial application.

2.6 Antibacterial properties of N-GQDs

For another kind of CDs which do not require photoexcitation to inhibit bacteria growth, they are commonly made from bottom-up process. [67, 68] Bottom up method enables a larger freedom of surface modification so that the CDs can kill target species with modified surface functional groups.

Nitrogen is a popular dopant because of the formation of cationic N-GQDs surface to interact with bacteria. Yang *et al.* demonstrated the antibacterial effect of amine-functionalized CDs on gram-positive bacteria. [67] The negatively charged teichoic acids on the peptidoglycan in cell membrane enable the electrostatic binding of the cationic surface of amine-functionalized CDs. The study of Bunz *et al.* showed that cationic Au NPs aggregated more on the surface of gram-positive *B. subtilis* than gram-negative *E. coli*, confirming the interaction between cationic NPs and gram-positive bacteria. There have been other reports showing amino group is closely related to the nanomaterial's antibacterial property. [30, 40, 69-72]

Chapter 3 Experimental Details

3.1 Microwave-Assisted Hydrothermal Synthesis

Microwave is a desirable heating source for hydrothermal synthesis of GQDs, due to its convenience and rapid uniform heating. Using microwave as heating source drastically reduces the reaction time and improves product yield, while at the same time enhancing the uniformity of the product.

For microwave-assisted hydrothermal synthesis of nanocrystals or nanoparticles, the pressure can be either ambient-pressure or high-pressure. Ambient-pressure hydrothermal synthesis can be achieved by heating with domestic microwave apparatus. Although it is low-cost and convenient, the uniformity of nanoparticle grown is low because of unstable experimental environment, not to mention that stirring is not available throughout the heating process. For the high-pressure hydrothermal process, oven or microwave can be applied as a heating source. The precursors were sealed or kept in a closed container to attain a high-pressure environment. The reaction temperature can be lower because of the high reaction rate under high pressure.

In this work, nitrogen-doped GQDs were prepared by the microwave-assisted hydrothermal method. 0.4 g of *p-phenylenediamine* was dissolved in 20 mL of deionized water to form an aqueous solution. The solution was put into a glass vial with

flexible vial cap and heated with CEM Discover SP Microwave Synthesizer, enabling a precise control in reaction temperature and pressure. The temperature, pressure and heating time were set to be 180°C, 180 psi and 10 minutes respectively. After the heating process, the solution turned from pale red to deep wine red, indicating the formation of GQDs. The solution was then cooled to room temperature, followed by a separation process with column chromatography. The detail of column chromatography will be discussed in Chapter 4.

3.2 Characterization Methodology

3.2.1 *Transmission electron microscopy (TEM)*

Transmission electron microscopy (TEM) enables a precise and direct characterization on nanoparticles. It provides detail information on nanoparticles' size, shape and lattice parameters. By applying extremely high accelerating voltage, high-speed electrons emitted from the electron gun will pass through the adjustable magnetic condenser lens system to focus on a desired position of the specimen. The image is formed when the electron beam further passes through the objective lens system and forms a real image on the fluorescent screen. JEOL JEM-2100F Electron Scanning Microscope operating at 200kV was used to characterize the GQDs samples.

3.2.2 *Photoluminescence*

Photoluminescence (PL) is an essential technique for nanoparticle characterization. Photons were shone onto the sample to excite the GQDs to a higher energy state by absorbing photons with appropriate wavelengths, which depends on bandgaps of the specimen. The PL emission spectrum can then be obtained. Edinburgh Instruments FLSP920 with a xenon arc lamp was used. The emission light was detected by a monochromator.

3.2.3 *UV-visible Absorbance*

The UV-visible absorbance spectrum of the GQDs can be obtained by Shimadzu UV-2550 UV-vis spectrophotometer. The measurement of the target sample (GQDs aqueous solution) and referencing sample (deionized water) were taken at the same time throughout the process. The absorbance can be calculated as follow,

$$\mathrm{A} = log_{10} \frac{I_o}{I}$$

where A is the absorbance of the target species, I_o is the transmitted intensity of the reference sample and I is the transmitted intensity of the target species.

3.2.4 *X-ray Photoelectron Spectroscopy (XPS)*

X-ray photoelectron spectroscopy (XPS) is a technique focusing on measuring surface elemental composition, chemical and electronic states of the material. The X-ray beam is irradiated to the specimen, at the same time the kinetic energy and number of electrons escaping from the surface of the material is measured. After analysis, information about the target material's surface can be obtained. The electron binding energy of the emitted electrons can be determined with experimentally measured emitted electron kinetic energy, shown as the following equation,

$$E_{binding} = E_{photon} - (E_{kinetic} + \Phi)$$

where $E_{binding}$ is the binding energy of the electron, E_{photon} is the known energy of the X-ray photons being used, $E_{kinetic}$ is the kinetic energy of the electron measured by the instrument and Φ is the work function depending on both spectrometer and the material. X-ray photoelectron spectrometer (Axis Ultra DLD system, Kratos Analytical, UK) equipped with a 150W monochromatic Al K_α X-ray source (1486.6eV) was adopted for the analysis.

3.2.5 *Fourier Transform infrared spectroscopy (FTIR)*

Fourier Transform Infrared Spectroscopy gives important information on surface bonding of the sample, making use of the absorption characteristic and natural vibration frequency in infrared range. FTIR analysis was carried out by Burker Vertex-70 FTIR with a resolution of 4 cm^{-1}. Infrared light beam is transmitted to the sample after passing through Michelson interferometer and finally received by IR detector. The IR photon will be absorbed by when the frequency of the IR photon matches the natural frequency of the molecules in the sample. The interferogram is obtained as a result of IR intensity against optical path difference. Hence, the interferogram is Fourier transformed into IR spectrum with transmittance against wave number in cm^{-1}.

3.2.6 *Atomic Force Microscopy (AFM)*

Atomic Force Microscopy (AFM) reveals the surface height profile of the GQDs. The atomic force between the sharp tip at the end of a flexible cantilever and sample surface was detected by the deflection of a laser directed to the cantilever by a photodetector. When the tip scans throughout the sample, the cantilever deflects due to the surface roughness, inducing the laser beam to deflect to a different position on the photodiode array. The variation in photocurrent generated determines the surface height profile of the sample. AFM in this report was measured by Digital Instrument NanoScope IV operating in tapping mode.

3.2.7 *Raman Spectroscopy*

Raman Spectroscopy is a technique to observe vibrational, rotational and low-energy modes. The sample is first illuminated with a laser beam. The light ray from the illuminated spot passes through a lens and a monochromator. The elastically scattered radiation at the wavelength corresponding to the laser line is filtered, and the remaining light is collected by a photodetector. The Raman spectroscopy was obtained by LabRAM HR 800.

3.2.8 *X-ray Diffraction (XRD)*

X-ray Diffraction (XRD) gives information of atomic and molecular structure of a crystal sample. Incident X-rays diffracts into many specific directions when it is irradiated onto the sample. By measuring the angles and intensities of the diffracted beam, information about the crystalline structure in the sample can be determined. XRD data was obtained by Rigaku SmartLab X-ray Diffractometer.

3.2.9 *Minimum Inhibitory Concentration (MIC)*

Minimum inhibitory concentration (MIC) is the lowest concentration of a chemical to inhibit visible growth of a bacteria specie. The chemical solution was prepared *in vitro* at various concentrations with separated batches. Same amount of target bacteria species was incubated with the batches for more than 10 hours. Optical transparency for the batch solution indicates the inhibitory ability of the chemical to the bacteria.

Susceptibility to nanoparticles and MICs were tested on *Staphylococcus aureus* and *Escherichia coli* strains using the standard broth dilution method as described by the Clinical and Laboratory Standards Institute. [73-75]

Chapter 4 Column Chromatography

Chromatography is a technique for separation of a mixture. The mixture is dissolved in a solvent which is called mobile phase. The mobile phase carries the sample through another adsorbent material called stationary phase. Individual specie in the sample moves at different rates depending on the solubility and polarity of the specie to achieve separation. There are various chromatography methodologies, like liquid column chromatography (LC), gas column chromatography (GC) and thin-layer chromatography (TLC), depending on the states and properties of the analyte.

4.1 Stationary phase and mobile phase

There are two phases involved in chromatography, mobile phase and stationary phase. The mobile phase (which is also called eluent) is an analyte mixture dissolved in a solvent, while the stationary phase is an adsorbent. The mobile phase can be a pure solvent or a mixture of different solvents.

The stationary phase in column chromatography is a solid, with porous polar surface and large effective surface area. The silica gel and alumina are two popular stationary phase candidates. Silica gel particles with a size of 40 - 63 μm are commonly used. The porous surface enables an effective physical adsorption of mobile phase onto it, making silica gel suitable as a stationary state. In this report, silica gel with sizes of 70 – 200 μm and pore size of 60 Å was chosen to be the stationary phase for separation

of N-GQDs sample.

Figure 4.1 illustrates the mechanism of liquid chromatography. The glass column filled with stationary phase and mobile phase. The organic solvent continuously flows downwards throughout the process. The analyte (a mixture to be separated) is drawn downwards by the solvent flow. The species in analyte may have different physical adsorption onto the polar stationary phase. Species with higher polarity would have higher adsorption power, and hence a slower travelling rate. Eventually, the species in the mixture can be separated by the difference in travelling rate due to their polarity difference.

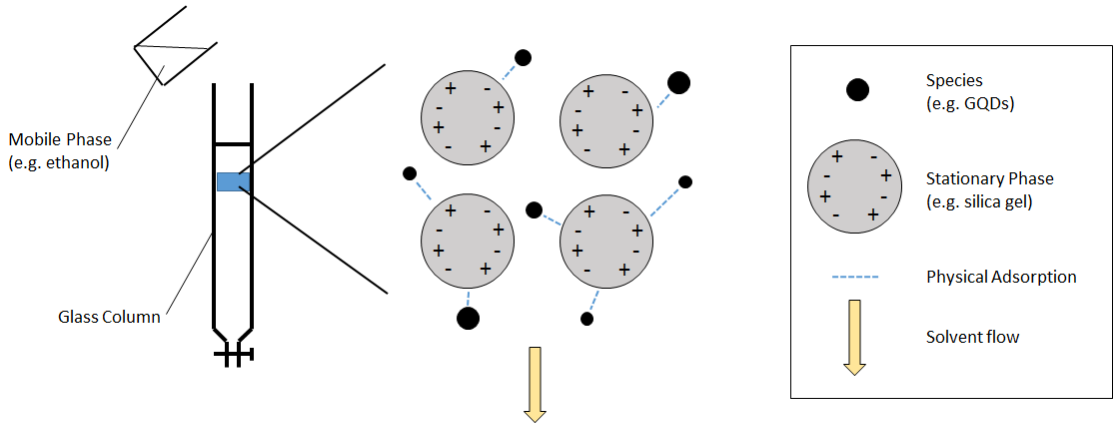

Figure 4.1 Schematic diagram illustrating the mechanism of LC

Figure 4.2 illustrates a typical LC process. The column is loaded with the stationary phase, followed by adding eluent. The mixture is then added to the top of the stationary phase. After that, the eluent is added constantly to prevent the stationary phase from drying. In Figure 4.2, the mixture is divided into two fractions, which is red

and blue in color. The red fraction moves at a rate faster than the blue fraction and is collected first.

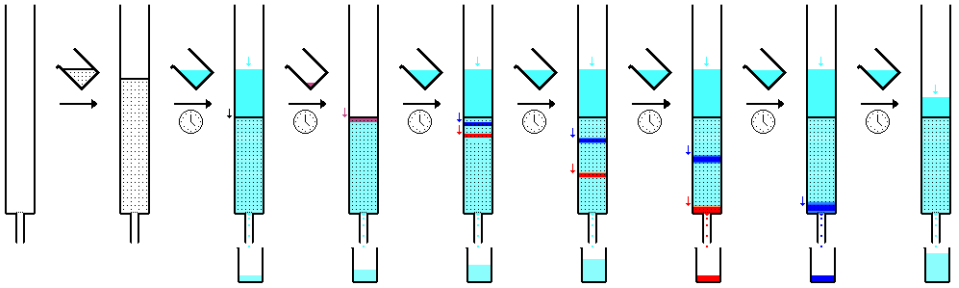

Figure 4.2 Schematic diagram illustrating the column chromatography process. [76]

Due to the polarity difference of the individual component in the analyte, difference in retention factor (k) is observed when they pass through the column, where retention factor is defined as

$$k = \frac{quantity\ \ of\ \ substance\ \ in\ \ the\ \ mobile\ \ phase}{total\ \ quantity\ \ of\ \ substance\ \ in\ \ the\ \ system}$$

The eluent with retention factor value of the analyte is chosen to be roughly around 0.2 – 0.3. The analyte travels too fast if the retention factor is too high so that the component will mix together and do not have enough time to be clearly separated in a high resolution. If a low retention factor is chosen, it consumes unnecessarily long time for the separation process. Besides, the stationary phase may be stacked more and more tightly throughout the process, further reducing the traveling speed of the analyte.

4.2 Significance of liquid chromatography

Since our N-GQDs was synthesized by hydrothermal method, the as-prepared product was a mixture of GQDs with variation in surface functional group, and hence the difference in polarity. Therefore, applying column chromatography enables an effective separation of GQDs mixture into more uniform GQD fractions.

Most importantly, liquid chromatography enables a fairer comparison on properties and performance among the separated fraction. There were reports studying the antibacterial ability of GQDs.[65, 67, 69, 77, 78] The GQDs were synthesized in various ways, with different structures and surface passivation. It is not preferable to compare their properties directly, as there are too many variables for the synthesized GQDs.

LC can separate a GQD mixture into various fraction according to their polarities, enabling a fairer investigation on the correlation between its surface functional group and the antibacterial power.

4.3 Thin-layer Chromatography (TLC)

Thin-layer chromatography (TLC) is an analytical chromatography technique used to separate the non-volatile mixture. It can be performed on a sheet of glass, plastic or aluminium foil coated with a thin layer of adsorbent material, acting as the stationary phase. TLC is usually done before running LC (liquid chromatography) to test whether the choice of stationary and mobile phase is suitable to make an effective separation.

The sample is first applied to the plate and dried, a solvent is then drawn up the plate by capillary action. Separation can be achieved because the component of analyte travels along the solvent-front at different rates. After the solvent-front has reached almost the top of the plate, the plate can be dried for clearer visualization of spots. Direct observation on spots can be done for colored components. Sheets can be treated with phosphor to visualize those invisible components by observing black spots, because of optical absorption due to the presence of species.

It is necessary to have an accurate quantification for the position and sequence component spots. Retardation factor (R_f) is a quantity indicating the distance travelled by each component. Definition of R_f is shown as follows,

$$R_f = \frac{migration\ \ distance\ \ of\ \ substance}{migration\ \ distance\ \ of\ \ solvent\ \ front}$$

Figure 4.3 shows the separation of the N-GQDs on a TLC plate (silica gel 60 F_{254} from EMD Millipore Corporation) with 1:6 ethanol and ethyl acetate as solvent. The

components go upwards with the solvent front when the TLC plate is dipped into the solvent. The N-GQDs mixture is separated into various fractions with color ranging from yellow brown, deep red, rose red to purple.

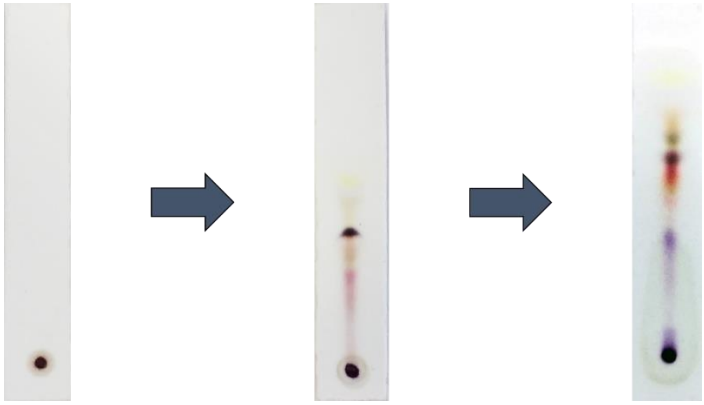

Figure 4.3 The movement of the N-GQD sample on a TLC aluminium plate with silica gel chosen as absorbent.

4.4 Liquid Column Chromatography (LC)

Liquid chromatography (LC) is a method to purify and separate chemical components from a mixture in a larger quantity than TLC. The major advantages of running column chromatography are the low cost and easy disposing of stationary phase after use. A glass column tube with diameter from millimeters to centimeters and length from centimeters to meters is used for the separation, depending on the samples size and analyte property. When the components are retained by the stationary phase differently, they reach the bottom of the column at different orders and can be collected fraction by fraction.

4.4.1 *Experimental Procedure*

A piece of cotton wool was first put at the inner bottom of the glass column to prevent silica gel from flowing into the collected sample. After that, the silica gel was mixed with ethyl acetate and poured into the glass column till the stationary phase level reaches about 80% of the glass column height. The silica gel sticking on the wall of the glass column was washed by adding ethyl acetate. As-prepared N-GQDs sample was dried and dissolved in 5 mL of 2:1 ethyl acetate and ethanol mixture. The N-GQDs solution was added to the top of slightly wet silica gel surface carefully. The tap was opened until the solvent level reached the silica gel level, then 2 mL of solvent was added. The above process was repeated for 10 times. After that, the solvent was added from time to time in order to prevent mobile phase from drying. Throughout the whole experiment, the polarity of the solvent is increased gradually by mixing ethyl acetate with ethanol to have a better separation quality. After all desired fractions were collected, the column was dried and the silica gel was disposed of.

Chapter 5 Characterization of N-GQDs

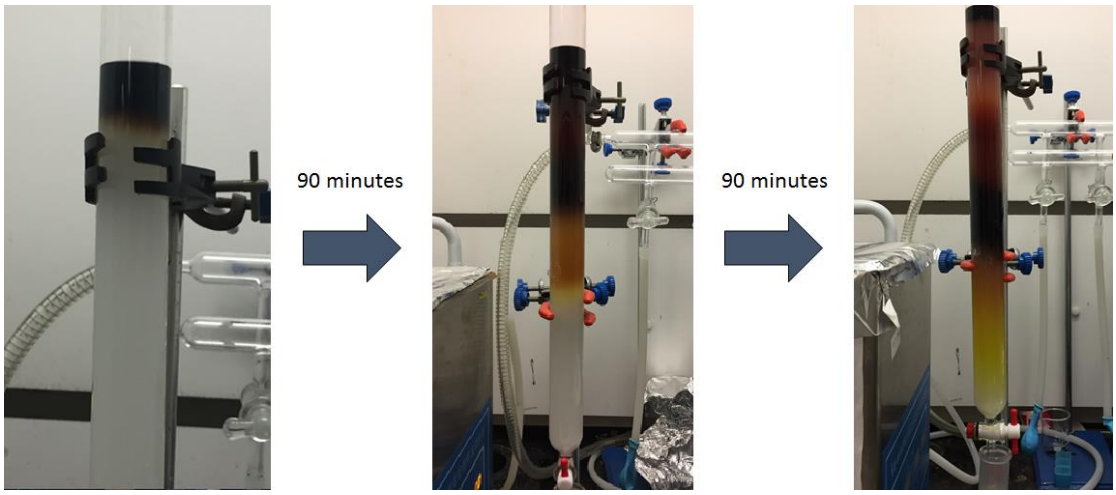

Figure 5.1 Photos showing various N-GQD fractions moving down the column as a function of time.

Figure 5.1 shows the column filled with silica gel and the N-GQDs travelling with different rates. The as-prepared GQD sample are placed at the top of the column. With continuous downward flow of the mobile phase, the GQD fractions travelled at different rates. The sample shows color varying from yellow, orange, brown to deep red under daylight. They are collected into four fractions according to their appearance.

5.1 Optical Properties

Figure 5.2a shows the PL spectra of the four GQD fractions dispersed in water. The excitation wavelengths of 340 nm, 460 nm, 480 nm and 500 nm were used to excite g-GQDs, y-GQDs, o-GQDs and r-GQDs respectively. The insets show the appearance of the GQD fraction under daylight. The four fractions are showing PL emission color in the order of green, yellow, orange and red. The four GQD fractions are labeled as g-GQDs, y-GQDs, o-GQDs and r-GQDs. The order indicates the increase in polarity of the GQDs from g-GQDs to r-GQDs, therefore a trend of more polar GQDs giving a longer emission wavelength is observed. The PL spectra of each individual fraction as a function of excitation wavelength are shown in Figure 5.3. Before the separation, the as-prepared GQDs shows an excitation independent PL with a peak emission at 630 nm. The g-GQDs and r-GQDs also exhibit an excitation independence with a peak emission at 540 nm and 630 nm respectively. The y-GQDs and o-GQDs exhibit a slight excitation dependence at around 520 nm and 590 nm under different excitation wavelengths.

Figure 5.2b shows the absorption spectrum of GQDs fractions. All the fractions show an absorption peak at 245 nm, indicating π-π* transitions of C=C bonds. The o-GQDs and r-GQDs show a significant absorption shoulder at 275 nm, indicating the π-π* transitions of C=N bonds. Besides, g-GQDs exhibit a strong blue absorption at 396 nm, while other fractions also show a slight absorption in visible range, indicating the

presence of various surface states due to passivation.

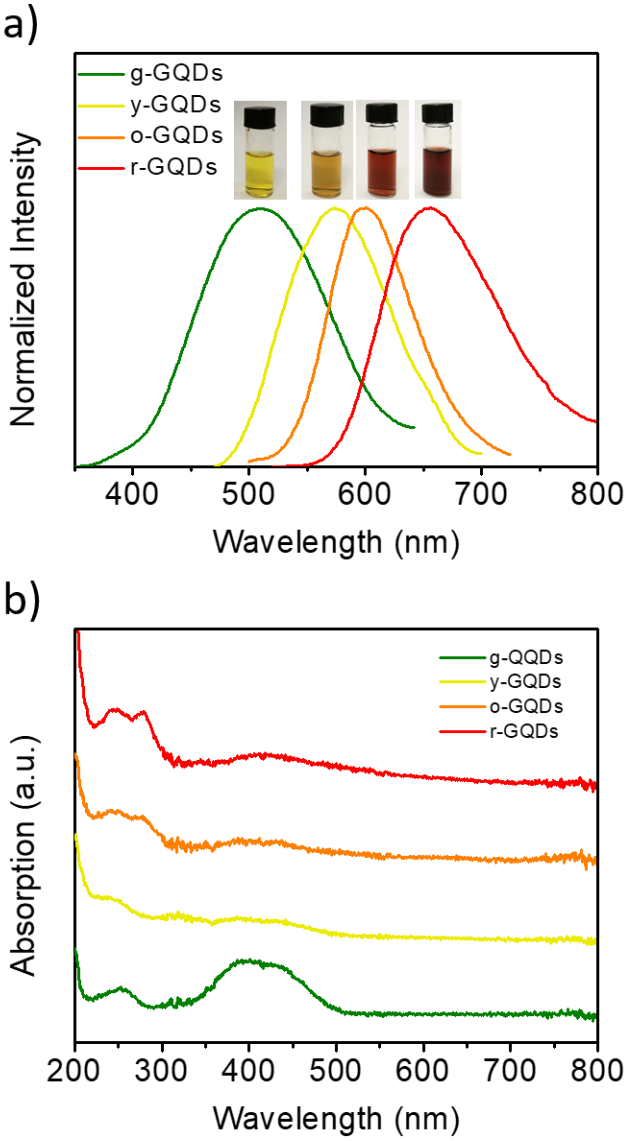

Figure 5.2 (a) The nominated PL emission spectra of the GQD fractions. Inset are the photos of the fractions. **(b)** Absorption spectra of the four GQD fractions.

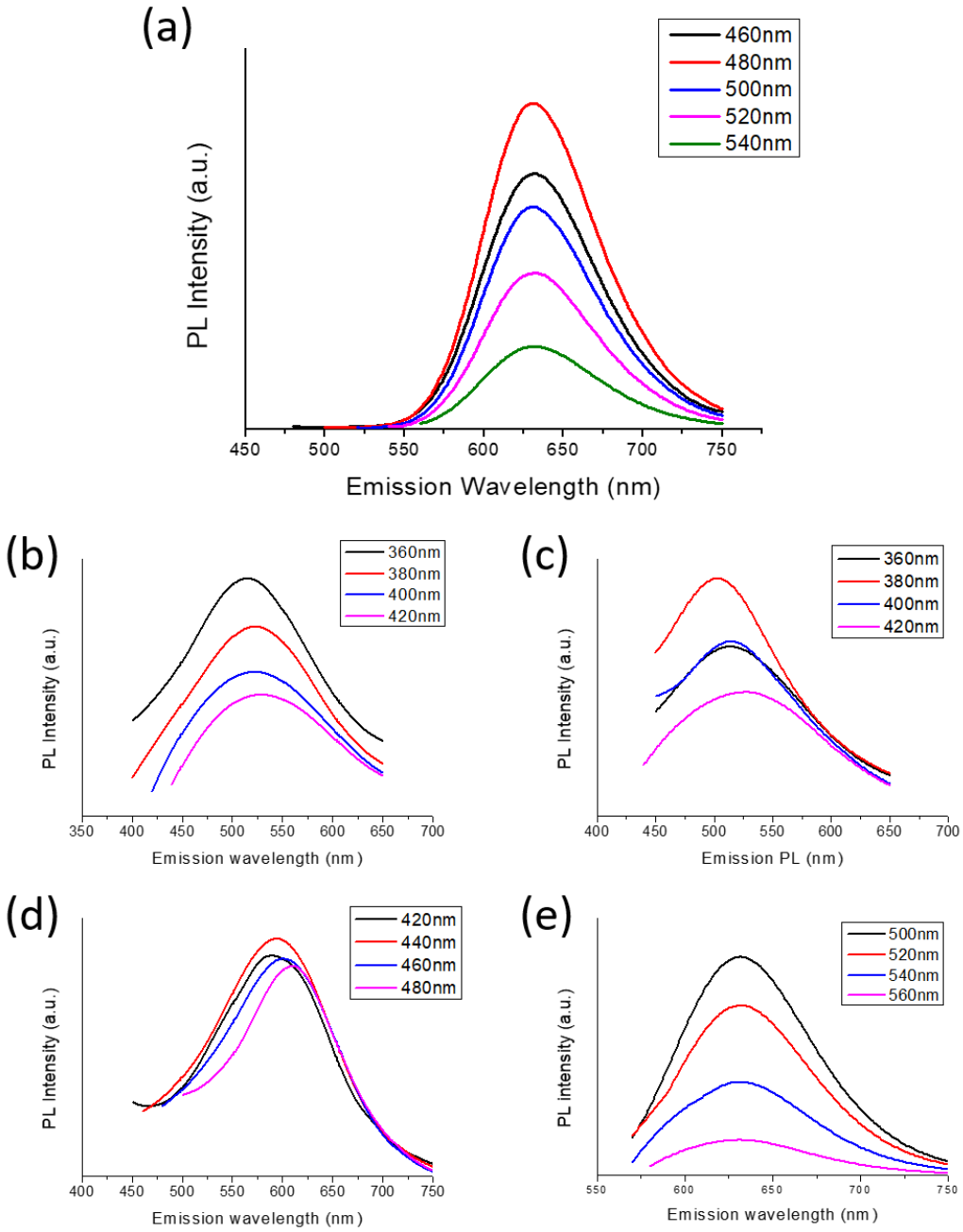

Figure 5.3 PL of the (a) GQDs before separation process, (b) g-GQDs, (c) o-GQDs, (d) y-GQDs, (e) r-GQDs under different excitation wavelengths.

5.2 Structural Properties

Figure 5.4 shows the TEM image of the four GQD fractions. The GQDs are well-dispersed and with a similar average particle size of approximately 2.5 nm. The size variation is small of about 2-3 nm in variation, as shown in Figure 5.5. The lattice fringe is observed to be 0.21 nm, which matched with the (100) lattice plane of graphene. [14] AFM image shows the height of the GQDs is from 1.5 to 2.5 nm, as shown in Figure 5.6. Thus, the average size of the GQDs in the four fractions are similar.

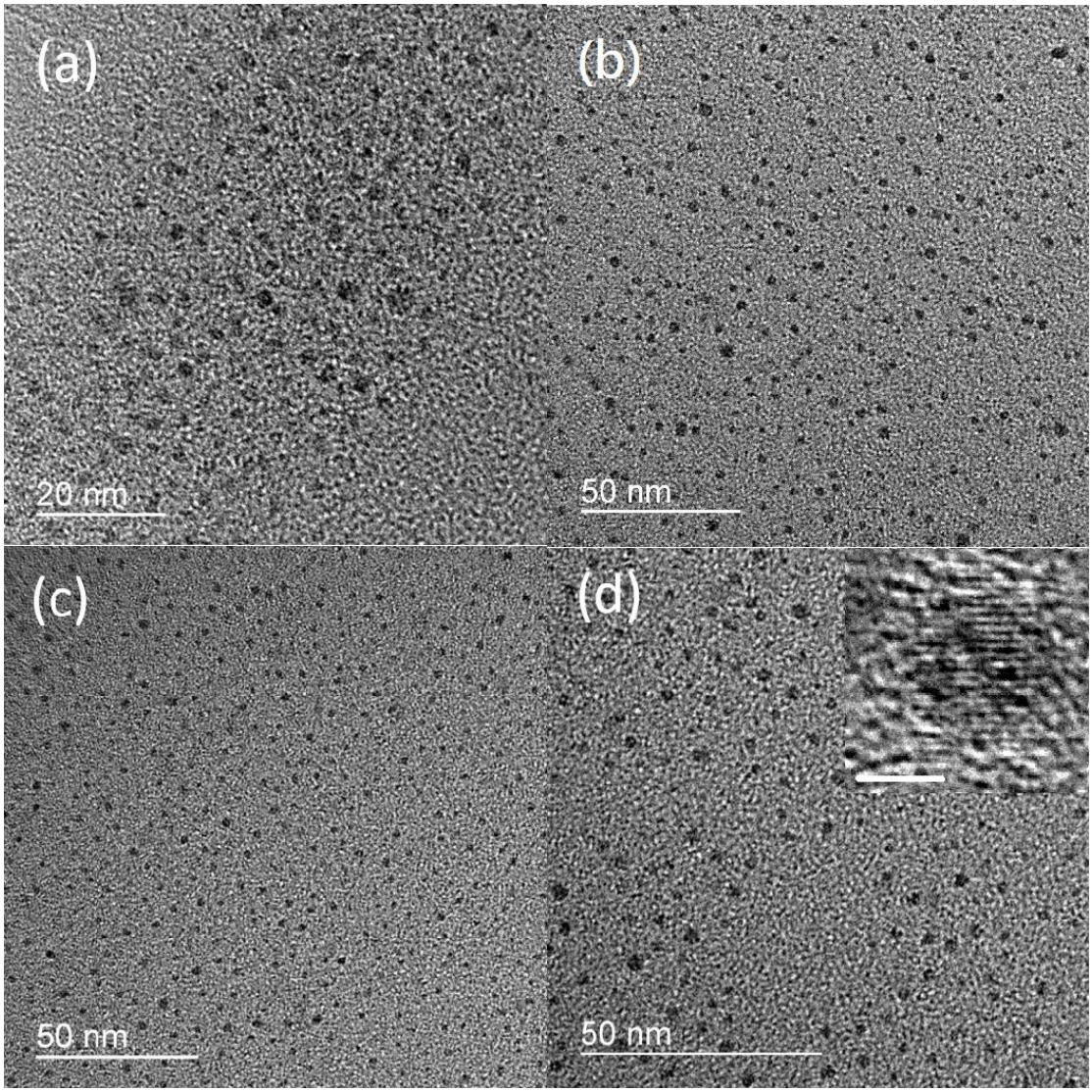

Figure 5.4 TEM images of the four GQD fractions, g-GQDs in **(a)**, y-GQDs in **(b)**, o-GQDs in **(c)**, r-GQDs in **(d)**. Lattice fringe of a single GQDs particle is shown in the inset of **(d)**, with the scale bar of 2 nm.

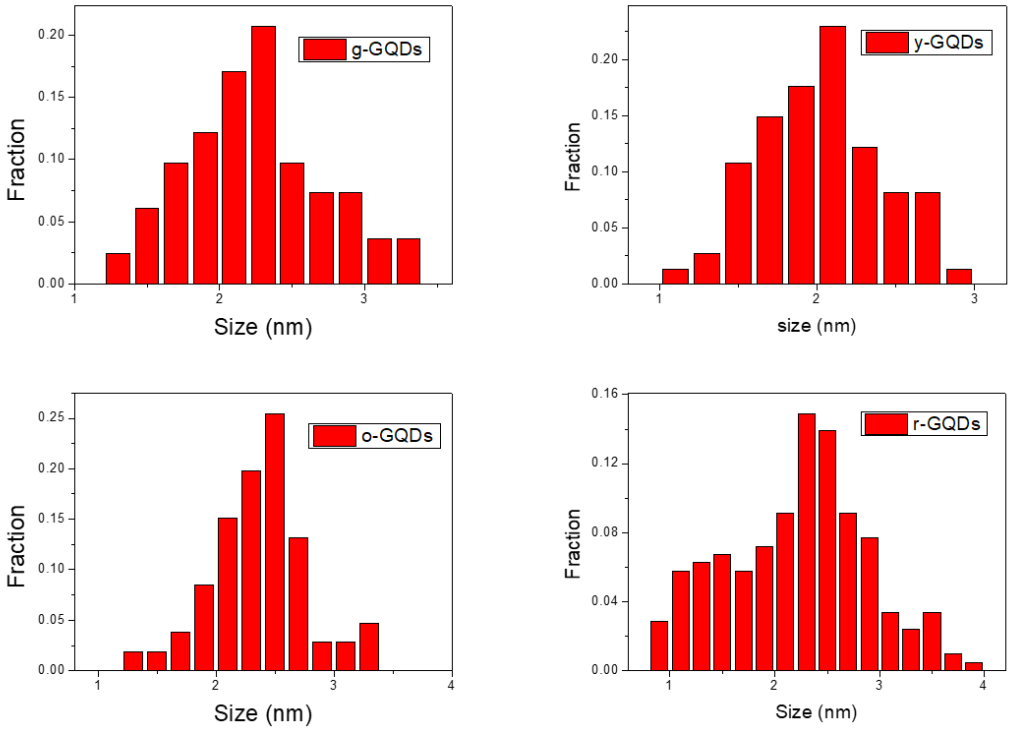

Figure 5.5 Size distribution of the four GQD fractions

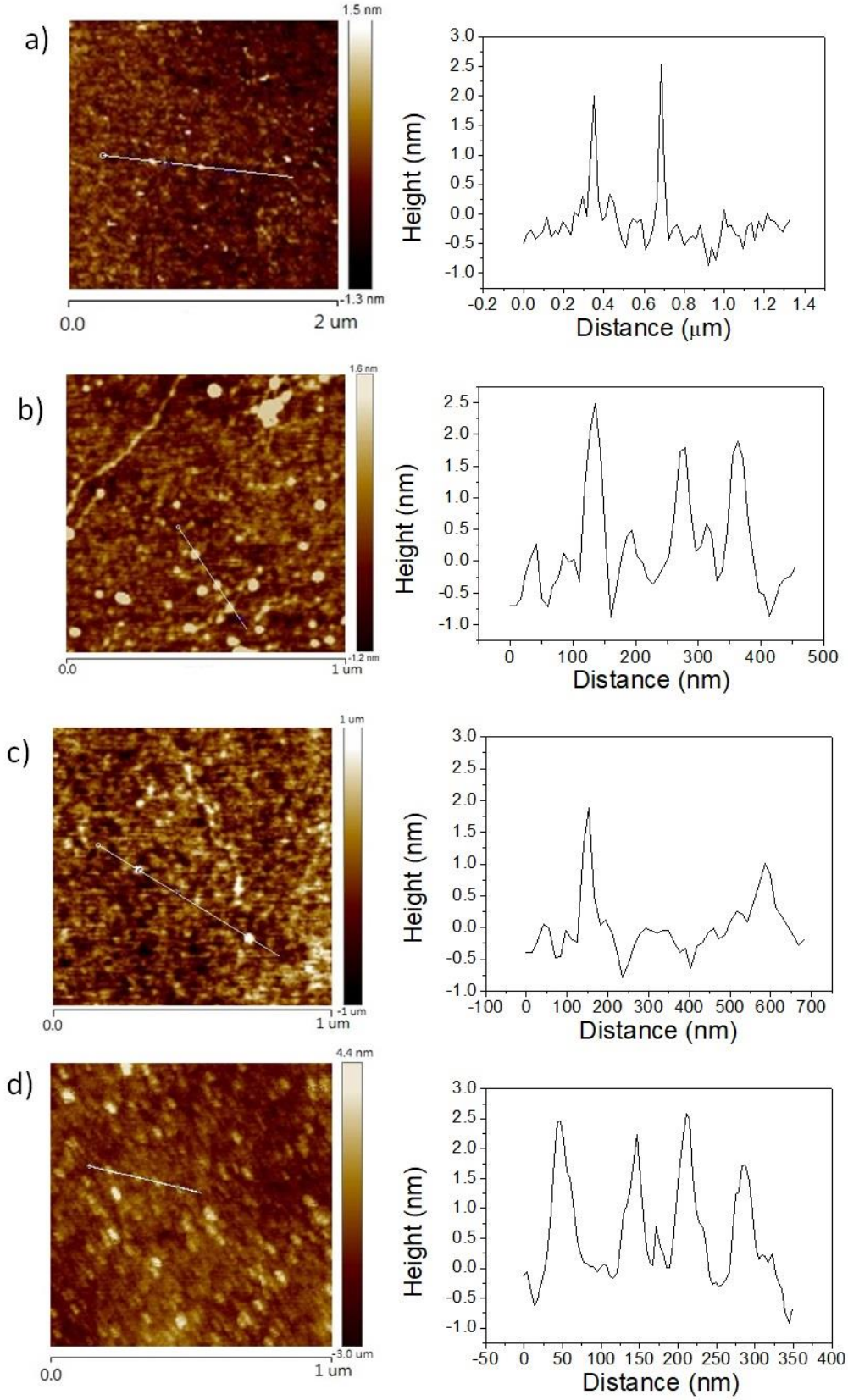

Figure 5.6 AFM height images of **(a)** g-GQDs, **(b)** o-GQDs, **(c)** y-GQDs, **(d)** r-GQDs

Figure 5.7 shows the XPS spectra of the four GQD fractions. There are C 1s (285eV), N 1s (400eV) and O 1s (531eV) peaks in all the fractions, showing the presence of carbon, nitrogen and oxygen bondings in the samples. Figure 5.8 shows the C 1s spectra of the GQD fractions. The spectra can be resolved into three peaks, which are at the positions of 284.4 eV (C-C/C=C), 285.3 eV (C-N) and 286.5 eV (C-O). Figure 5.9 shows the N 1s spectra of the GQD fractions. The spectra can be resolved into three peaks, which are located at 398.0 eV (pyridinic N), 399.1 eV (amino N) and 400.2 eV (pyrrolic N).

The intensity of the O 1s peak decreases from g-GQDs to r-GQDs, indicating a decreasing trend of oxygen content (from 13.5% to 7.15%) as shown in Table 5.1. On the other hand, the intensity of the N 1s peak increases from g-GQDs to r-GQDs, indicating an increasing trend of nitrogen content (9.12% to 16.18%).

Table 5.2 reveals the percentage content of pyridinic N, amino N and pyrrolic N in the four fractions. It is found that amino N content significantly increases from g-GQDs to r-GQDs (from 15.5% to 68.8%), while pyridinic N and pyrrolic N decreases.

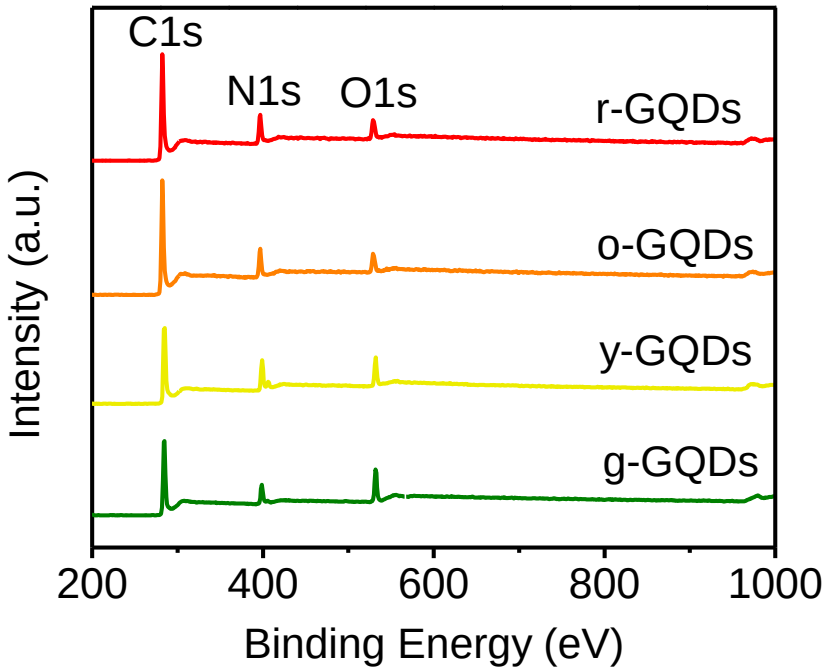

Figure 5.7 Full range XPS spectra of the four GQD fractions.

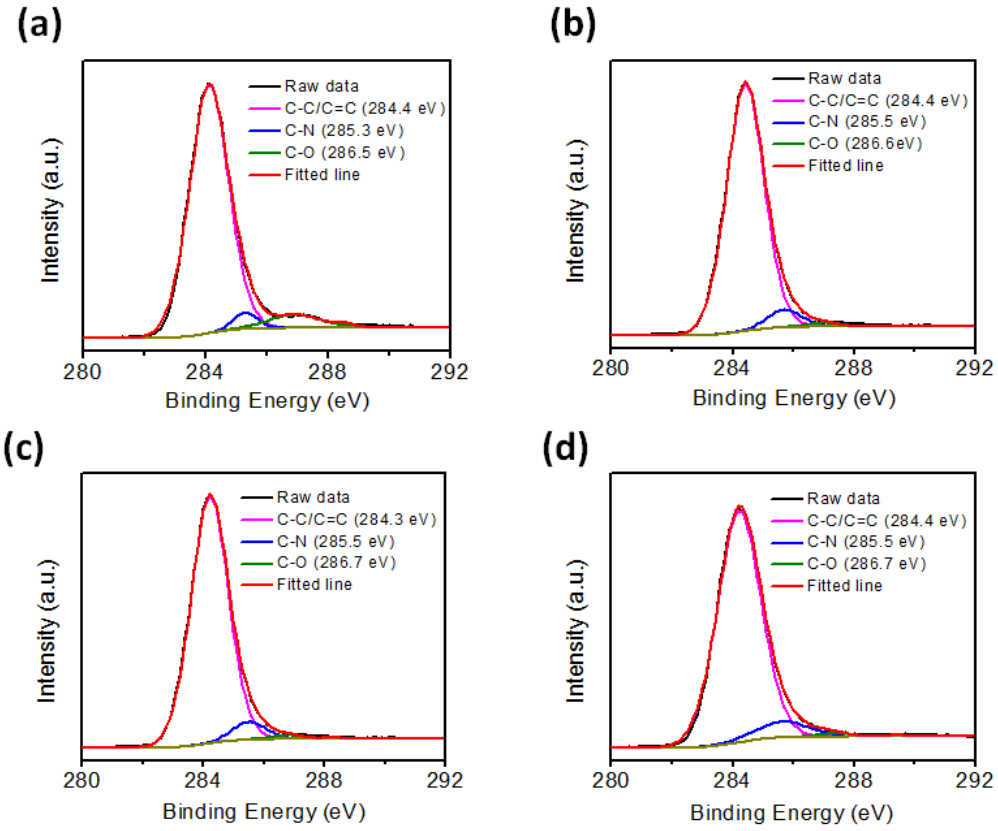

Figure 5.8 XPS C 1s spectra of the (a) g-GQDs, (b) y-GQDs, (c) o-GQDs, (d) r-GQDs.

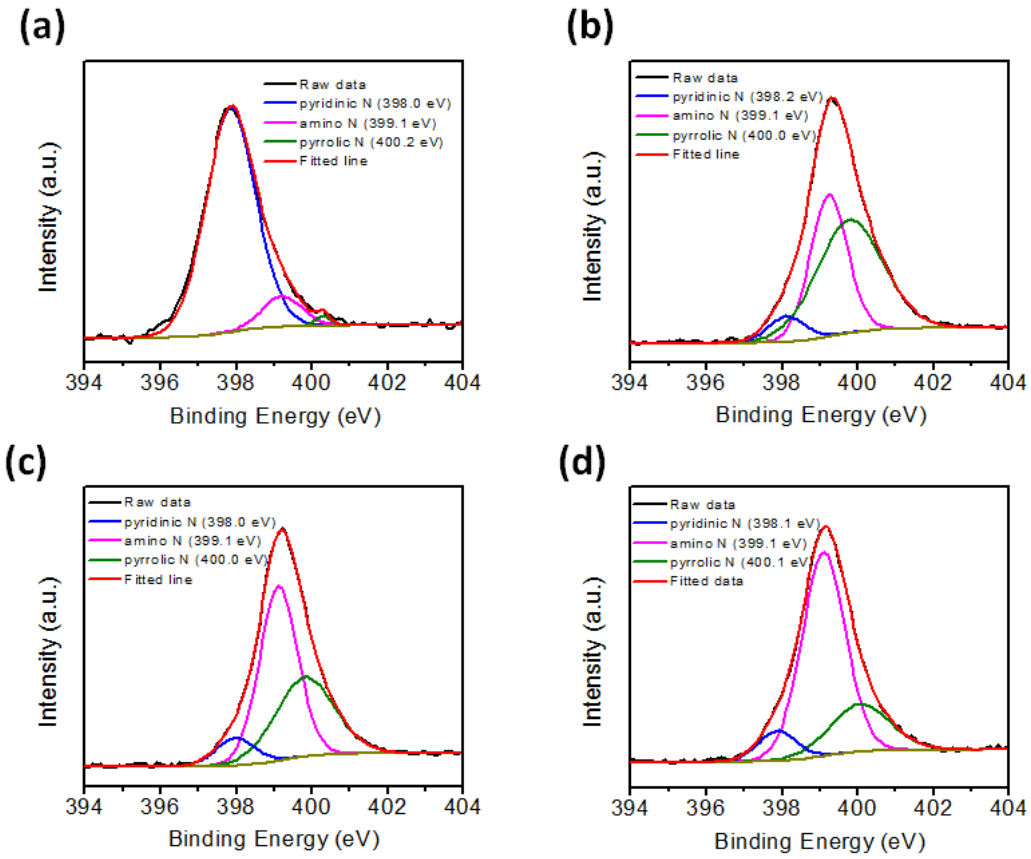

Figure 5.9 XPS N 1s spectra of the (a) g-GQDs, (b) y-GQDs, (c) o-GQDs, (d) r-GQDs.

Fraction	C atomic percentage (%)	N atomic percentage (%)	O atomic percentage (%)
g-GQDs	77.38	9.12	13.50
y-GQDs	77.80	12.10	10.10
o-GQDs	77.22	14.57	8.21
r-GQDs	76.67	16.18	7.15

Table 5.1 Atomic percentage content of the GQD fractions

Fraction	Pyridinic N (%)	Amino N (%)	Pyrrolic N (%)
r-GQDs	79.2	15.5	5.3
y-GQDs	9.6	41.2	49.2
o-GQDs	10.5	59.3	30.2
r-GQDs	11.1	68.8	20.1

Table 5.2 XPS data analysis by resolving N 1s peak of the GQD fractions

The Fourier transform infrared (FTIR) spectra of the GQD fractions were measured to investigate the bonding composition. The result is shown in Figure 5.10. The GQD fractions possess nitrogen and oxygen bonding like C-O (1259 cm^{-1}), C-N (1417 cm^{-1}), N-H (1610 cm^{-1} and 3188 cm^{-1}) and O-H (3360 cm^{-1}). Besides, C=C (1496 cm^{-1}), is also present, showing the graphitic structure of the GQDs. There is one important message revealed from the FTIR spectra of the amino content. The stretching vibration of N-H at 1610 cm^{-1} is enhanced from g-GQDs to r-GQDs, showing the increasing amino content in the respective fractions, on the basis that N-H bond can only be present in amino group. The information is consistent with the result obtained from XPS.

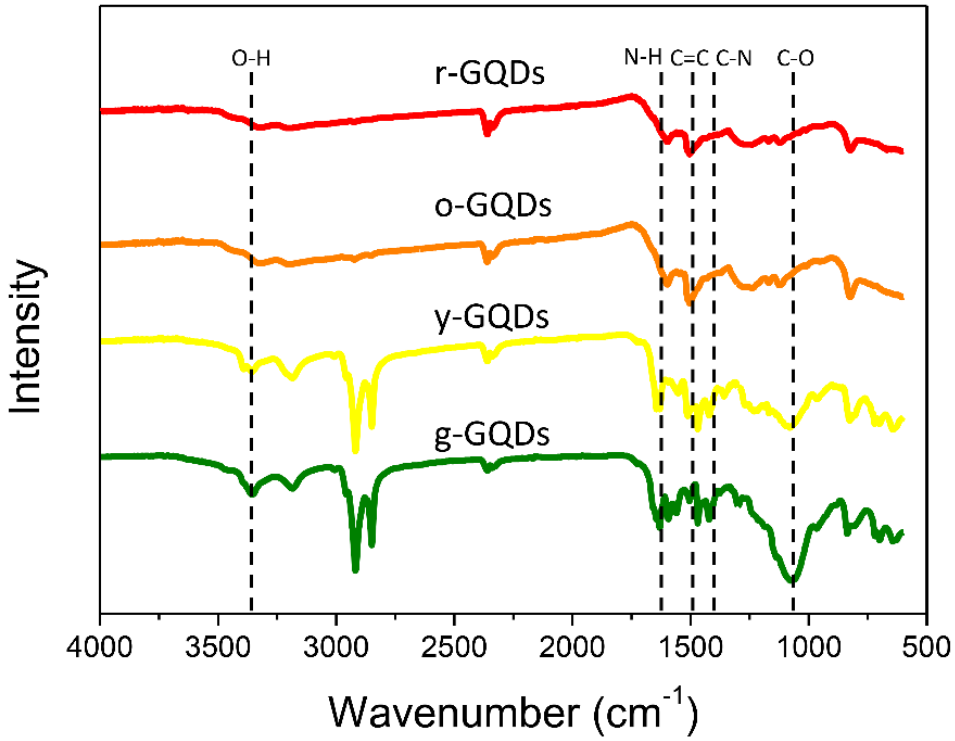

Figure 5.10 FTIR spectra of the GQD fractions.

The Raman spectra of the four GQD fractions are shown in Figure 5.11. The D band at 1350 cm^{-1} and G band at 1595 cm^{-1} are obvious, indicating the presence of graphitic structure defects. The broad D band suggests that some carbon atoms are intercalated as substitution of carbon atom in the graphitic structure. The I_D/I_G ratio was found to be varying between 0.60 and 0.76, suggesting the GQD fractions are defect-rich. The X-ray diffraction (XRD) patterns of the GQDs (Figure 5.12) show consistent peaks at 23°, corresponding to a graphitic structure. Because of the presence of internal defects and oxygen or nitrogen functional groups like –O–H, –N–H_2 and –C–O–R, the GQDs were enlarged in different degree, causing the bandwidth of XRD pattern to be

broad.

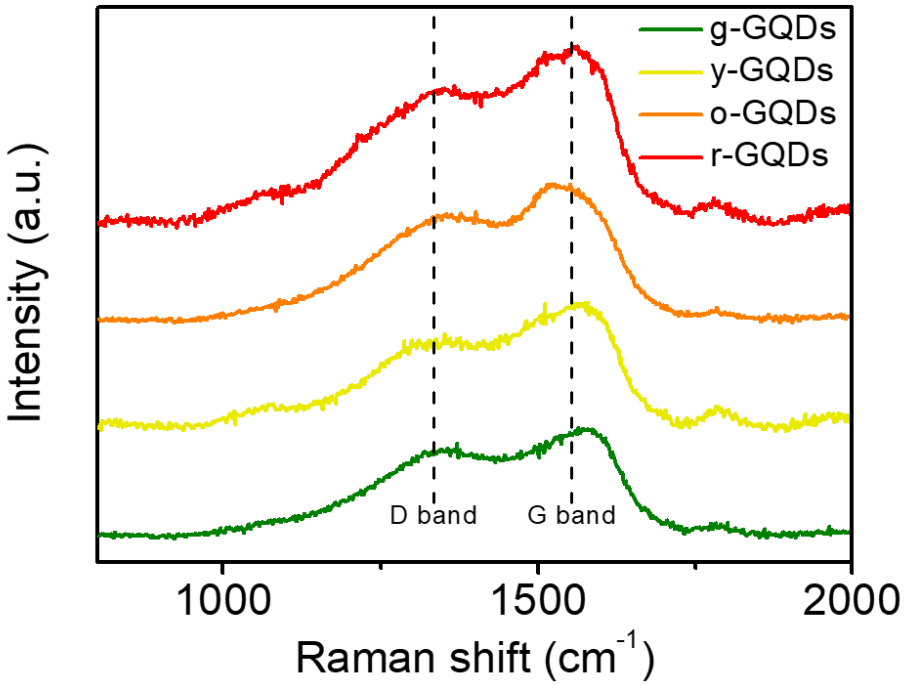

Figure 5.11 Raman spectra of the GQD fractions.

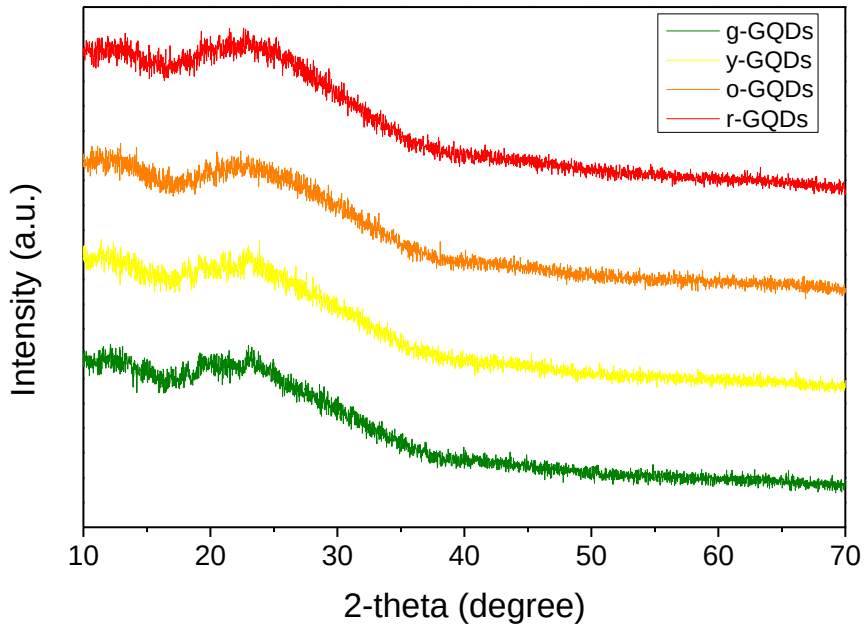

Figure 5.12 XRD pattern of the GQD fractions

Chapter 6 Antibacterial Property of N-GQDs

6.1 Minimal Inhibitory Concentration (MIC)

Minimal inhibitory concentration (MIC) test was carried out to identify the antibacterial property of the GQDs. It is defined as the lowest concentration of certain antimicrobial agent that can inhibit the growth of a bacteria. Table 6.1 summarizes the MIC values of the four GQD fractions on gram-positive *S. aureus* and gram-negative *E. coli.* It is found that the MIC value of the four fractions towards *S. aureus* has a decreasing trend from g-GQDs (171 μg/mL) to r-GQDs (43 μg/mL), indicating a lower concentration is needed to inhibit the growth of *S. aureus*, and hence an increasing antibacterial power against *S. aureus*. MIC values of the GQDs on *E. coli.* is relatively larger, of more than 128 μg/mL. The antibacterial power of the GQDs is higher against *S. aureus* than *E. coli.*

Fraction	*S. aureus*	*E. coli*
g-GQDs	171	>256
y-GQDs	107	>256
o-GQDs	85	128
r-GQDs	43	128

Table 6.1 MIC values of the GQDs fractions against *S. aureus* and *E. coli.* (unit: μg/mL)

Previous reports demonstrated that the bacterial inhibiting effect of nitrogen functional groups on carbon materials. However, no investigation on the relationship between nitrogen content and the antibacterial effect was carried out. [67-69, 71, 72] In this work, we found that the amino functional group could be associated with the antibacterial power of the GQDs.

As shown in the XPS characterization, the nitrogen content increases from g-GQDs to r-GQDs. Interestingly, the antibacterial power towards *S. aureus* increases from g-GQDs to r-GQDs. The MIC result reveals that the nitrogen content of the GQDs may play a role in the antibacterial property.

Besides, it should be noted that most of the nitrogen atoms comes from amino groups. Figure 6.1 shows the relationship between the amino N content of the GQD fractions and their MIC value. It shows that an increasing surface amino N content gives a lower MIC value linearly. Therefore, the amino group could be an active functional group for its antibacterial power.

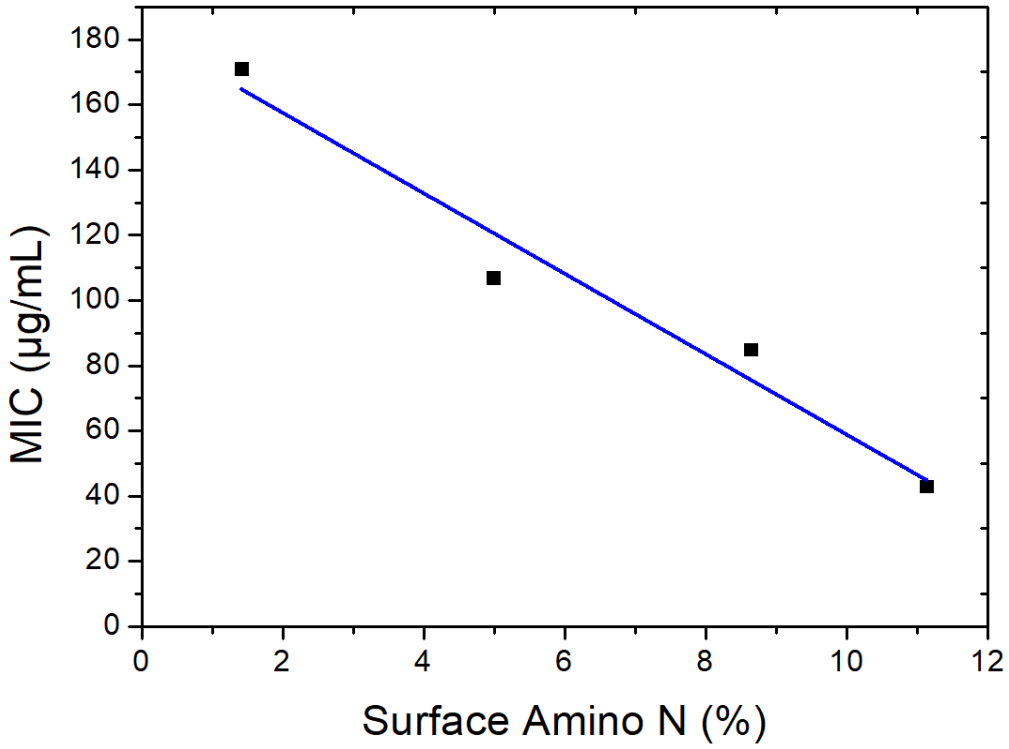

Figure 6.1 Plot of the MIC value as a function of amino N content.

Chapter 7 Conclusion and Future Works

7.1 Conclusion

In conclusion, GQDs have been successfully synthesized by microwave-assisted hydrothermal method. Nucleation of *p-phenylenediamine* under high pressure and temperature formed nitrogen-doped GQDs. Column chromatography was applied to the GQD sample to separate them into four fractions (g-GQDs, y-GQDs, o-GQDs and r-GQDs) accordingly to their photoluminescence emission. The fractions show different physical and optical properties. XPS characterization shows the variation of nitrogen content from 9.12% to 16.2% among the fractions.

Gram-positive *S. aureus* and gram-negative *E. coli* were treated with the GQD fractions. It is found that the GQD fractions possess a higher inhibiting power on *S. aureus* than *E.coli*. MIC tests showed that GQD fractions with higher nitrogen content possess a stronger inhibiting power on *S. aureus*.

7.2 Future Works

In this work, a relationship between nitrogen content (especially amino group) in the GQDs and its antibacterial power is revealed. Additional works are required to enhance the antibacterial ability of GQDs further. The actual antibacterial mechanism has yet to be verified. The development of synthesis methods to incorporate high content of amino group into GQDs is needed. Further exploration of GQDs may open the door to a new-age drug development.

Reference

[1] K. Hola, Y. Zhang, Y. Wang, E. P. Giannelis, R. Zboril, and A. L. Rogach, "Carbon dots-Emerging light emitters for bioimaging, cancer therapy and optoelectronics,", *Nano Today,* Review vol. 9, no. 5, pp. 590-603, Oct 2014.

[2] C. Y. Chen *et al.*, "Highly responsive MoS_2 photodetectors enhanced by graphene quantum dots,", *Scientific Reports,* Article vol. 5, p. 9, Jul 2015, Art. no. 11830.

[3] H. Tetsuka, A. Nagoya, T. Fukusumi, and T. Matsui, "Molecularly Designed, Nitrogen-Functionalized Graphene Quantum Dots for Optoelectronic Devices," *Advanced Materials,* vol. 28, no. 23, pp. 4632-4638, 2016.

[4] L. B. Tang *et al.*, "Deep Ultraviolet to Near-Infrared Emission and Photoresponse in Layered N-Doped Graphene Quantum Dots,", *Acs Nano,* Article vol. 8, no. 6, pp. 6312-6320, Jun 2014.

[5] C. M. Luk, L. B. Tang, W. F. Zhang, S. F. Yu, K. S. Teng, and S. P. Lau, "An efficient and stable fluorescent graphene quantum dot-agar composite as a converting material in white light emitting diodes,", *Journal of Materials Chemistry,* Article vol. 22, no. 42, pp. 22378-22381, Nov 2012.

[6] S. H. Song *et al.*, "Highly Efficient Light-Emitting Diode of Graphene Quantum Dots Fabricated from Graphite Intercalation Compounds,", *Advanced Optical Materials,* Article vol. 2, no. 11, pp. 1016-1023, Nov 2014.

[7] K. J. Williams, C. A. Nelson, X. Yan, L. S. Li, and X. Y. Zhu, "Hot Electron Injection from Graphene Quantum Dots to TiO2,", *Acs Nano,* Article vol. 7, no. 2, pp. 1388-1394, Feb 2013.

[8] Q. Zhang *et al.*, "Solution-Processed Graphene Quantum Dot Deep-UV Photodetectors,", *Acs Nano,* Article vol. 9, no. 2, pp. 1561-1570, Feb 2015.

[9] Y. Li *et al.*, "An Electrochemical Avenue to Green-Luminescent Graphene Quantum Dots as Potential Electron-Acceptors for Photovoltaics,", *Advanced Materials,* Article vol. 23, no. 6, pp. 776-+, Feb 2011.

[10] X. Yan, X. Cui, B. S. Li, and L. S. Li, "Large, Solution-Processable Graphene Quantum Dots as Light Absorbers for Photovoltaics,", *Nano Letters,* Article vol. 10, no. 5, pp. 1869-1873, May 2010.

[11] I. Mihalache *et al.*, "Charge and energy transfer interplay in hybrid sensitized solar cells mediated by graphene quantum dots,", *Electrochimica Acta,* Article vol. 153, pp. 306-315, Jan 2015.

[12] M. L. Tsai *et al.*, "Si Hybrid Solar Cells with 13% Efficiency via Concurrent Improvement in Optical and Electrical Properties by Employing Graphene Quantum Dots,", *Acs Nano,* Article vol. 10, no. 1, pp. 815-821, Jan 2016.

[13] L. M. Zhang *et al.*, "Preparation of Graphene Quantum Dots for Bioimaging Application,", *Journal of Nanoscience and Nanotechnology,* Article vol. 12, no. 3, pp. 2924-2928, Mar 2012.

[14] H. Ding, S. B. Yu, J. S. Wei, and H. M. Xiong, "Full-Color Light-Emitting Carbon Dots with a Surface-State-Controlled Luminescence Mechanism,", *Acs Nano,* Article vol. 10, no. 1, pp. 484-491, Jan 2016.

[15] L. Wang *et al.*, "Facile synthesis of fluorescent graphene quantum dots from coffee grounds for bioimaging and sensing,", *Chemical Engineering Journal,* Article vol. 300, pp. 75-82, Sep 2016.

[16] N. Abdullah Al *et al.*, "Target Delivery and Cell Imaging Using Hyaluronic Acid-Functionalized Graphene Quantum Dots,", *Molecular Pharmaceutics,* Article vol. 10, no. 10, pp. 3736-3744, Oct 2013.

[17] H. J. Sun, H. W. Ji, E. G. Ju, Y. J. Guan, J. S. Ren, and X. G. Qu, "Synthesis of Fluorinated and Nonfluorinated Graphene Quantum Dots through a New Top-Down Strategy for Long-Time Cellular Imaging,", *Chemistry-a European Journal,* Article vol. 21, no. 9, pp. 3791-3797, Feb 2015.

[18] Q. Liu, B. D. Guo, Z. Y. Rao, B. H. Zhang, and J. R. Gong, "Strong Two-Photon-Induced Fluorescence from Photostable, Biocompatible Nitrogen-Doped Graphene Quantum Dots for Cellular and Deep-Tissue Imaging,", *Nano Letters,* Article vol. 13, no. 6, pp. 2436-2441, Jun 2013.

[19] J. C. Ge *et al.*, "Red-Emissive Carbon Dots for Fluorescent, Photoacoustic, and Thermal Theranostics in Living Mice,", *Advanced Materials,* Article vol. 27, no. 28, pp. 4169-4177, Jul 2015.

[20] L. Li, G. Wu, G. Yang, J. Peng, J. Zhao, and J.-J. Zhu, "Focusing on luminescent graphene quantum dots: current status and future perspectives," *Nanoscale,* 10.1039/C3NR33849E vol. 5, no. 10, pp. 4015-4039, 2013.

[21] K. S. Novoselov *et al.*, "Electric field effect in atomically thin carbon films,", *Science,* Article vol. 306, no. 5696, pp. 666-669, Oct 2004.

[22] G. Eda *et al.*, "Blue Photoluminescence from Chemically Derived Graphene Oxide,", *Advanced Materials,* Article vol. 22, no. 4, pp. 505-+, Jan 2010.

[23] L. B. Tang *et al.*, "Deep Ultraviolet Photoluminescence of Water-Soluble Self-Passivated Graphene Quantum Dots,", *Acs Nano,* Article vol. 6, no. 6, pp. 5102-5110, Jun 2012.

[24] S. K. Das *et al.*, "Size and Dopant Dependent Single Particle Fluorescence Properties of Graphene Quantum Dots,", *Journal of Physical Chemistry C,* Article vol. 119, no. 31, pp. 17988-17994, Aug 2015.

[25] L. B. Tang, R. B. Ji, X. M. Li, K. S. Teng, and S. P. Lau, "Energy-level structure of nitrogen-doped graphene quantum dots,", *Journal of Materials Chemistry C,*

Article vol. 1, no. 32, pp. 4908-4915, 2013.

[26] L. Q. Lu, Y. C. Zhu, C. Shi, and Y. T. T. Pei, "Large-scale synthesis of defect-selective graphene quantum dots by ultrasonic-assisted liquid-phase exfoliation,", *Carbon,* Article vol. 109, pp. 373-383, Nov 2016.

[27] Y. H. Zhu, G. F. Wang, H. Jiang, L. Chen, and X. J. Zhang, "One-step ultrasonic synthesis of graphene quantum dots with high quantum yield and their application in sensing alkaline phosphatase,", *Chemical Communications,* Article vol. 51, no. 5, pp. 948-951, 2015.

[28] Z. Y. Li, W. H. Zhang, Y. Luo, J. L. Yang, and J. G. Hou, "How Graphene Is Cut upon Oxidation?,", *Journal of the American Chemical Society,* Article vol. 131, no. 18, pp. 6320-+, May 2009.

[29] J. Peng *et al.*, "Graphene Quantum Dots Derived from Carbon Fibers,", *Nano Letters,* Article vol. 12, no. 2, pp. 844-849, Feb 2012.

[30] H. Tetsuka *et al.*, "Optically Tunable Amino-Functionalized Graphene Quantum Dots,", *Advanced Materials,* Article vol. 24, no. 39, pp. 5333-5338, Oct 2012.

[31] S. Y. Ju, W. P. Kopcha, and F. Papadimitrakopoulos, "Brightly Fluorescent Single-Walled Carbon Nanotubes via an Oxygen-Excluding Surfactant Organization,", *Science,* Article vol. 323, no. 5919, pp. 1319-1323, Mar 2009.

[32] J. Lu, J. X. Yang, J. Z. Wang, A. L. Lim, S. Wang, and K. P. Loh, "One-Pot Synthesis of Fluorescent Carbon Nanoribbons, Nanoparticles, and Graphene by the Exfoliation of Graphite in Ionic Liquids,", *Acs Nano,* Article vol. 3, no. 8, pp. 2367-2375, Aug 2009.

[33] J. G. Zhou *et al.*, "An electrochemical avenue to blue luminescent nanocrystals from multiwalled carbon nanotubes (MWCNTs),", *Journal of the American Chemical Society,* Article vol. 129, no. 4, pp. 744-745, Jan 2007.

[34] J. Lu, P. S. E. Yeo, C. K. Gan, P. Wu, and K. P. Loh, "Transforming C60 molecules into graphene quantum dots," *Nat Nano,* 10.1038/nnano.2011.30 vol. 6, no. 4, pp. 247-252, 04//print 2011.

[35] Y. X. Huang, X. C. Dong, Y. X. Liu, L. J. Li, and P. Chen, "Graphene-based biosensors for detection of bacteria and their metabolic activities,", *Journal of Materials Chemistry,* Article vol. 21, no. 33, pp. 12358-12362, 2011.

[36] R. Sekiya, Y. Uemura, H. Murakami, and T. Haino, "White-Light-Emitting Edge-Functionalized Graphene Quantum Dots," *Angewandte Chemie,* vol. 126, no. 22, pp. 5725-5729, 2014.

[37] Y. Dong *et al.*, "One-step and high yield simultaneous preparation of single- and multi-layer graphene quantum dots from CX-72 carbon black," *Journal of Materials Chemistry,* 10.1039/C2JM30658A vol. 22, no. 18, pp. 8764-8766,

2012.

[38] M. Zhang *et al.*, "Facile synthesis of water-soluble, highly fluorescent graphene quantum dots as a robust biological label for stem cells," *Journal of Materials Chemistry,* 10.1039/C2JM16835A vol. 22, no. 15, pp. 7461-7467, 2012.

[39] M. Shehab, S. Ebrahim, and M. Soliman, "Graphene quantum dots prepared from glucose as optical sensor for glucose," *Journal of Luminescence,* vol. 184, pp. 110-116, 4// 2017.

[40] Y. H. Li, H. B. Shu, X. H. Niu, and J. L. Wang, "Electronic and Optical Properties of Edge-Functionalized Graphene Quantum Dots and the Underlying Mechanism,", *Journal of Physical Chemistry C,* Article vol. 119, no. 44, pp. 24950-24957, Nov 2015.

[41] S. Wang, I. S. Cole, D. Zhao, and Q. Li, "The dual roles of functional groups in the photoluminescence of graphene quantum dots," *Nanoscale,* 10.1039/C5NR07042B vol. 8, no. 14, pp. 7449-7458, 2016.

[42] L. Zhang, Z. Y. Zhang, R. P. Liang, Y. H. Li, and J. D. Qiu, "Boron-Doped Graphene Quantum Dots for Selective Glucose Sensing Based on the "Abnormal" Aggregation-Induced Photoluminescence Enhancement,", *Analytical Chemistry,* Article vol. 86, no. 9, pp. 4423-4430, May 2014.

[43] D. Pan, J. Zhang, Z. Li, C. Wu, X. Yan, and M. Wu, "Observation of pH-, solvent-, spin-, and excitation-dependent blue photoluminescence from carbon nanoparticles," *Chemical Communications,* 10.1039/C000114G vol. 46, no. 21, pp. 3681-3683, 2010.

[44] Z.-A. Qiao *et al.*, "Commercially activated carbon as the source for producing multicolor photoluminescent carbon dots by chemical oxidation," *Chemical Communications,* 10.1039/C0CC02724C vol. 46, no. 46, pp. 8812-8814, 2010.

[45] H. Li, Z. Kang, Y. Liu, and S.-T. Lee, "Carbon nanodots: synthesis, properties and applications," *Journal of Materials Chemistry,* 10.1039/C2JM34690G vol. 22, no. 46, pp. 24230-24253, 2012.

[46] H. T. Li *et al.*, "Water-Soluble Fluorescent Carbon Quantum Dots and Photocatalyst Design,", *Angewandte Chemie-International Edition,* Article vol. 49, no. 26, pp. 4430-4434, 2010.

[47] S. J. Zhu *et al.*, "Surface Chemistry Routes to Modulate the Photoluminescence of Graphene Quantum Dots: From Fluorescence Mechanism to Up-Conversion Bioimaging Applications,", *Advanced Functional Materials,* Article vol. 22, no. 22, pp. 4732-4740, Nov 2012.

[48] S. Zhuo, M. Shao, and S.-T. Lee, "Upconversion and Downconversion Fluorescent Graphene Quantum Dots: Ultrasonic Preparation and

Photocatalysis," *ACS Nano,* vol. 6, no. 2, pp. 1059-1064, 2012/02/28 2012.

[49] Y. H. Li, H. B. Shu, S. D. Wang, and J. L. Wang, "Electronic and Optical Properties of Graphene Quantum Dots: The Role of Many-Body Effects,", *Journal of Physical Chemistry C,* Article vol. 119, no. 9, pp. 4983-4989, Mar 2015.

[50] X. M. Li, S. P. Lau, L. B. Tang, R. B. Ji, and P. Z. Yang, "Multicolour light emission from chlorine-doped graphene quantum dots,", *Journal of Materials Chemistry C,* Article vol. 1, no. 44, pp. 7308-7313, 2013.

[51] X. M. Li, S. P. Lau, L. B. Tang, R. B. Ji, and P. Z. Yang, "Sulphur doping: a facile approach to tune the electronic structure and optical properties of graphene quantum dots,", *Nanoscale,* Article vol. 6, no. 10, pp. 5323-5328, 2014.

[52] Y. Q. Zhang *et al.*, "One-pot synthesis of N-doped carbon dots with tunable luminescence properties,", *Journal of Materials Chemistry,* Article vol. 22, no. 33, pp. 16714-16718, 2012.

[53] M. J. Hajipour *et al.*, "Antibacterial properties of nanoparticles,", *Trends in Biotechnology,* Review vol. 30, no. 10, pp. 499-511, Oct 2012.

[54] WHO, "Antimicrobial Resistance,"

[55] A. J. Alanis, "Resistance to antibiotics: Are we in the post-antibiotic era?,", *Archives of Medical Research,* Review vol. 36, no. 6, pp. 697-705, Nov-Dec 2005.

[56] W. Jiang, H. Mashayekhi, and B. S. Xing, "Bacterial toxicity comparison between nano- and micro-scaled oxide particles,", *Environmental Pollution,* Article vol. 157, no. 5, pp. 1619-1625, May 2009.

[57] Y. H. Tsuang, J. S. Sun, Y. C. Huang, C. H. Lu, W. H. S. Chang, and C. C. Wang, "Studies of photokilling of bacteria using titanium dioxide nanoparticles,", *Artificial Organs,* Article vol. 32, no. 2, pp. 167-174, Feb 2008.

[58] K. Feris *et al.*, "Electrostatic Interactions Affect Nanoparticle-Mediated Toxicity to Gram-Negative Bacterium Pseudomonas aeruginosa PAO1," *Langmuir,* vol. 26, no. 6, pp. 4429-4436, 2010/03/16 2010.

[59] A. Kumar, A. K. Pandey, S. S. Singh, R. Shanker, and A. Dhawan, "Cellular uptake and mutagenic potential of metal oxide nanoparticles in bacterial cells,", *Chemosphere,* Article vol. 83, no. 8, pp. 1124-1132, May 2011.

[60] M. R. Hamblin *et al.*, "Nanotechnology for photodynamic therapy: a perspective from the Laboratory of Dr. Michael R. Hamblin in the Wellman Center for Photomedicine at Massachusetts General Hospital and Harvard Medical School,", *Nanotechnology Reviews,* Article vol. 4, no. 4, pp. 359-372, Aug 2015.

[61] W. S. Kuo *et al.*, "Two-Photon Photoexcited Photodynamic Therapy and

Contrast Agent with Antimicrobial Graphene Quantum Dots,", *Acs Applied Materials & Interfaces,* Article vol. 8, no. 44, pp. 30467-30474, Nov 2016.

[62] W.-S. Kuo *et al.*, "Graphene quantum dots with nitrogen-doped content dependence for highly efficient dual-modality photodynamic antimicrobial therapy and bioimaging," *Biomaterials,* vol. 120, pp. 185-194, 3// 2017.

[63] Z. M. Markovic *et al.*, "Graphene quantum dots as autophagy-inducing photodynamic agents,", *Biomaterials,* Article vol. 33, no. 29, pp. 7084-7092, Oct 2012.

[64] Y. Chong *et al.*, "Crossover between Anti- and Pro-oxidant Activities of Graphene Quantum Dots in the Absence or Presence of Light,", *Acs Nano,* Article vol. 10, no. 9, pp. 8690-8699, Sep 2016.

[65] M. J. Meziani *et al.*, "Visible-Light-Activated Bactericidal Functions of Carbon "Quantum" Dots,", *Acs Applied Materials & Interfaces,* Article vol. 8, no. 17, pp. 10761-10766, May 2016.

[66] J. C. Ge *et al.*, "A graphene quantum dot photodynamic therapy agent with high singlet oxygen generation,", *Nature Communications,* Article vol. 5, p. 8, Aug 2014, Art. no. 4596.

[67] J. Yang *et al.*, "Carbon Dot-Based Platform for Simultaneous Bacterial Distinguishment and Antibacterial Applications," *ACS Applied Materials & Interfaces,* vol. 8, no. 47, pp. 32170-32181, 2016/11/30 2016.

[68] Q. Dou, X. Fang, S. Jiang, P. L. Chee, T.-C. Lee, and X. J. Loh, "Multi-functional fluorescent carbon dots with antibacterial and gene delivery properties," *RSC Advances,* 10.1039/C5RA07968C vol. 5, no. 58, pp. 46817-46822, 2015.

[69] H. Z. Zardini, A. Amiri, M. Shanbedi, M. Maghrebi, and M. Baniadam, "Enhanced antibacterial activity of amino acids-functionalized multi walled carbon nanotubes by a simple method," *Colloids and Surfaces B: Biointerfaces,* vol. 92, pp. 196-202, 2012/04/01/ 2012.

[70] G. R. Bardajee, Z. Hooshyar, and F. Jafarpour, "Antibacterial and optical properties of a new water soluble CdSe quantum dots coated by multidentate biopolymer,", *Journal of Photochemistry and Photobiology a-Chemistry,* Article vol. 252, pp. 46-52, Jan 2013.

[71] M. J. Genin *et al.*, "Substituent Effects on the Antibacterial Activity of Nitrogen−Carbon-Linked (Azolylphenyl)oxazolidinones with Expanded Activity Against the Fastidious Gram-Negative Organisms Haemophilus influenzae and Moraxella catarrhalis," *Journal of Medicinal Chemistry,* vol. 43, no. 5, pp. 953-970, 2000/03/01 2000.

[72] X. Cai *et al.*, "The use of polyethyleneimine-modified reduced graphene oxide as a substrate for silver nanoparticles to produce a material with lower

cytotoxicity and long-term antibacterial activity," *Carbon,* vol. 50, no. 10, pp. 3407-3415, 2012/08/01/ 2012.

[73] L. L. Ling *et al.*, "A new antibiotic kills pathogens without detectable resistance," *Nature,* Article vol. 517, no. 7535, pp. 455-459, 01/22/print 2015.

[74] CLSI, Methods for Dilution Antimicrobial Susceptibility Tests for Bacteria That Grow Aerobically, 2012. [Online]. Available.

[75] CLSI, Performance Standards for Antimicrobial Susceptibility Testing；Twenty-sixth informational supplement, 2016. [Online]. Available.

[76] quantockgoblin. (2008). *Column chromatography Sequence*. Available: https://commons.wikimedia.org/w/index.php?curid=1603838

[77] B. Z. Ristic *et al.*, "Photodynamic antibacterial effect of graphene quantum dots,", *Biomaterials,* Article vol. 35, no. 15, pp. 4428-4435, May 2014.

[78] Q. Q. Dou, X. T. Fang, S. Jiang, P. L. Chee, T. C. Lee, and X. J. Loh, "Multi-functional fluorescent carbon dots with antibacterial and gene delivery properties,", *Rsc Advances,* Article vol. 5, no. 58, pp. 46817-46822, 2015.